Late Miocene–Pliocene range growth in the interior of the northeastern Tibetan Plateau

William Craddock[1,*], Eric Kirby[1], and Huiping Zhang[2]
[1]DEPARTMENT OF GEOSCIENCES, PENNSYLVANIA STATE UNIVERSITY, UNIVERSITY PARK, PENNSYLVANIA 16802, USA
[2]STATE KEY LABORATORY OF EARTHQUAKE DYNAMICS, INSTITUTE OF GEOLOGY, CHINA EARTHQUAKE ADMINISTRATION, BEIJING 100029, CHINA

ABSTRACT

The time-space patterns of deformation throughout the Indo-Asian collision zone can place constraints on the processes responsible for the development of high topography. Although most agree that high topography associated with the Tibetan Plateau expanded throughout the Cenozoic, it is increasingly being recognized that portions of the present-day plateau experienced a protracted history of deformation starting before or shortly after collision. Deciphering the history of deformation in these regions is central to understanding the dynamics of plateau formation. Here, we report new constraints on the timing of shortening along the southern margin of the Gonghe Basin complex, a broad Tertiary–Quaternary depocenter within the interior region of the northeastern Tibetan Plateau. Deformation of basin strata, lithostratigraphic patterns, and changes in paleocurrents record the growth of structures along the southern margin of the basin. A novel combination of magnetostratigraphy and cosmogenic burial ages from fluvial deposits provides a chronology that suggests that sediment accumulation initiated at ca. 20 Ma and that indicates the basin-bounding structures became active during the late Miocene, between ca. 10 and 7 Ma. The probable onset of basin development in the early Miocene is similar to other regions of the northeastern Tibetan Plateau, and it appears to herald the onset of widespread contractional deformation in the region. Moreover, late Miocene activity on thrusts bounding the southern margin of Gonghe Basin was broadly synchronous with the rise of mountain ranges elsewhere along the periphery of the plateau, suggesting a coordinated pulse of growth of high topography during this time.

LITHOSPHERE; v. 3; no. 6; p. 420–438; Data Repository Item 2011351. doi: 10.1130/L159.1

INTRODUCTION

The space-time patterns of deformation throughout the Indo-Asian collision zone provide first-order bounds on the processes responsible for the development of the thickened crust and high topography that characterize the modern-day Tibetan Plateau (Molnar et al., 1993; Royden et al., 2008). Initial collision of India with Eurasia occurred ca. 50 Ma (Garzanti and van Haver, 1988; Rowley, 1996; Najman et al., 2010) and near ~20°N latitude (Patriat and Achache, 1984; Dupont-Nivet et al., 2010), implying nearly ~3000 km of postcollision convergence (Dupont-Nivet et al., 2010). The ways in which this convergence has been accommodated, both within the Himalaya (e.g., DeCelles et al., 2002) and throughout the Eurasian lithosphere (e.g., Lippert et al., 2010), have driven a generation of research into the timing and magnitude of upper-crustal shortening (England and Houseman, 1986; Tapponnier et al., 2001; Molnar, 2005, and references therein). Collectively, these studies suggest that the southern margin of Eurasia was characterized by thickened crust (e.g., Murphy et al., 1997; Kapp et al., 2005) prior to collision, that high elevations in central and southern Tibet were achieved relatively quickly following collision (DeCelles et al., 2007; Rowley and Currie, 2006), and that deformation and crustal thickening progressed outward to the north and east from this elevated core (Meyer et al., 1998; Tapponnier et al., 2001; Royden et al., 2008).

Despite the consensus on this broad pattern, the timing of deformation and the growth of topography within the northeastern Tibetan Plateau is debated. Early workers held that growth of the Qilian Shan and associated ranges north and east of the Qaidam Basin (Fig. 1) was largely confined to the late Miocene and Pliocene (e.g., Burchfiel et al., 1989; Tapponnier et al., 1990, 2001; Meyer et al., 1998). Indeed, subsequent studies provided abundant evidence for mountain building throughout the northeastern Tibetan Plateau during late Miocene time (e.g., Zheng et al., 2003, 2006, 2010; Fang et al., 2005, 2007; Lease et al., 2007, 2011). Temporal coincidence in the onset of mountain building around the peripheral regions of Tibet has been suggested to reflect a fundamental change in the geodynamics of the collision zone (Molnar, 2005), perhaps related to an increase in potential energy associated with removal of mantle lithosphere beneath the plateau (Molnar and Stock, 2009). However, recent studies suggest that the history of mountain building may have been more complex. In particular, proxy evidence for a period of deformation in the early-mid Tertiary along the margins of the western Qaidam Basin (e.g., Ritts et al., 2004; Yin et al., 2008a, 2008b) and within northeastern Tibet (Fang et al., 2003; Dupont-Nivet et al., 2004, 2008; Clark et al., 2010; Duvall et al., 2011) has led some to consider that the present-day boundaries of the Tibetan Plateau were largely established at or near the onset of collision (Dayem et al., 2009).

Although these studies clearly suggest a protracted history of deformation and mountain building in northeastern Tibet, they leave open several outstanding questions regarding the timing of plateau growth. First, how widespread was the region of early Tertiary deformation? Were early Tertiary depocenters in western Qaidam linked with early Tertiary basins of the northeastern Tibetan Plateau (e.g., Clark et al., 2010), or did these regions evolve as separate tectonic elements (e.g., Wang et al., 2006)? Second, does the episode of mountain building in the late Miocene exhibit space-time patterns that may yield insight into proximate causes? Was range growth coordinated, reflecting northward propagation of deformation from the plateau (e.g., Meyer et al., 1998), or did ranges grow

*Current address: U.S. Geological Survey, MS 956, Reston, Virginia 20192, USA.

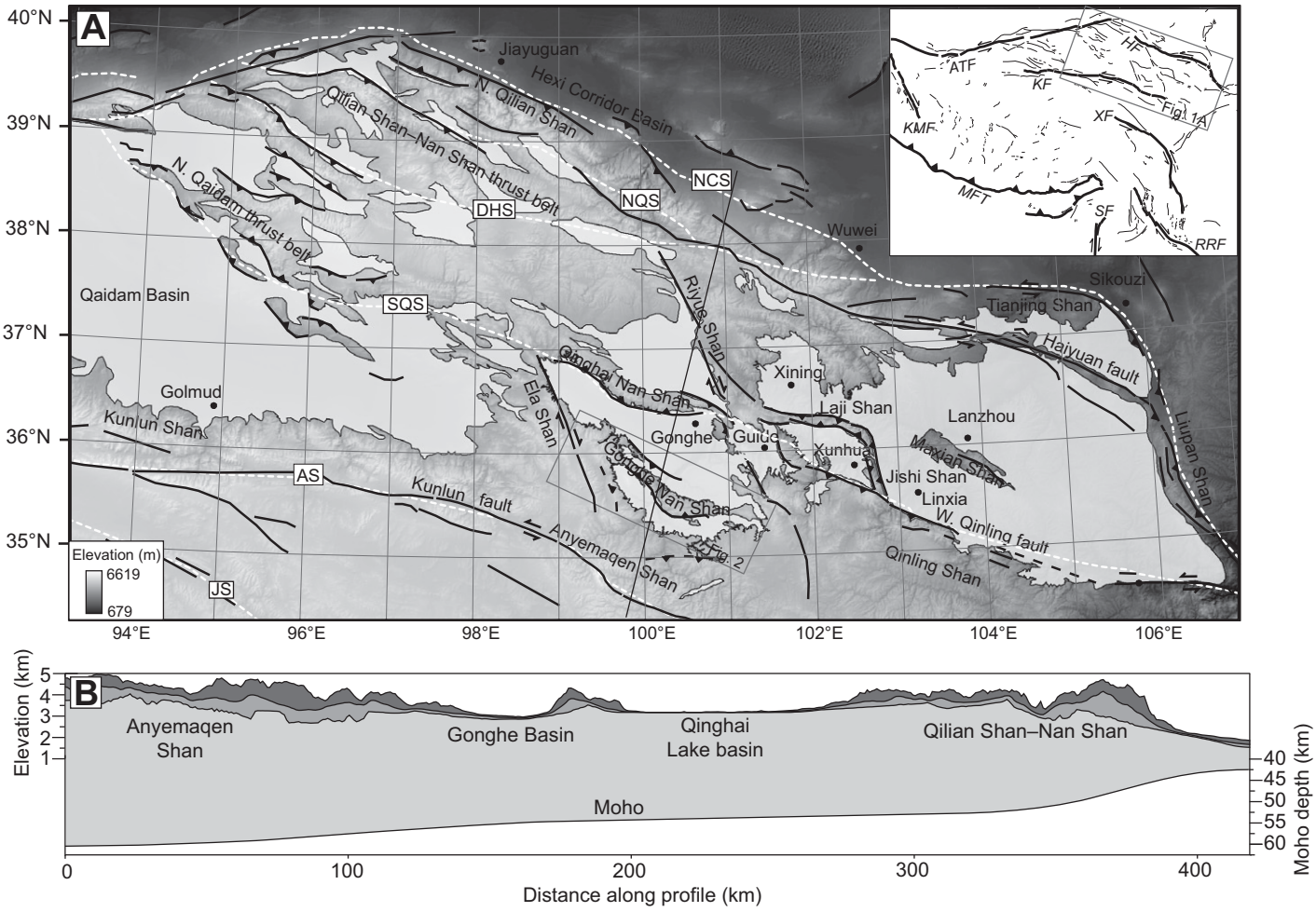

Figure 1. (A) Quaternary faults and Cenozoic basins in northern Tibet. Inset also shows Quaternary faults of the Tibetan Plateau. Topography is from GTOPO-30. Faults are adapted from Tapponnier and Molnar (1977); Molnar and Tapponnier (1978). ATF—Altyn Tagh fault, HF—Haiyuan fault, KF—Kunlun fault, KMF—Karakoram fault, MFT—Main Frontal thrust fault, RRF—Red River fault, SF—Saigang fault, XF—Xianshuihe fault. White dashed lines are terrane boundaries. AS—Anyemaqen suture, DHS—Danghe Nan Shan suture, JS—Jinsha suture, NCS—North China suture, NQS—North Qilian suture, SQS—South Qilian suture. Terrane boundaries are adapted from Yin and Harrison (2000), and Xiao et al. (2009), and references therein. (B) Maximum, minimum, and mean swath topography, derived from GTOPO-30 data, which have a nominal resolution of 1 km. Moho depths from the Anyemaqen and Gonghe are from Vergne et al. (2002), and depths from the Qilian Shan are from Meyer et al. (1998). Location of cross section corresponds to gray line oriented NNE across center of A.

asynchronously (e.g., Sobel et al., 2003), reflecting the disruption of a previously unbroken foreland (e.g., Strecker et al., 2007)? Here, we address these questions through detailed study of range growth along the southern margin of the Gonghe Basin, in interior northeastern Tibet.

The Gonghe Basin complex is located along the axis separating early Tertiary depocenters of the northeastern Tibetan Plateau from the Qaidam Basin, and thus the depositional history of this region provides a key test of the regional extent of early Tertiary sedimentation. Similarly, the basin sits today at a physiographic transition between the basin-and-range topography of the Qilian Shan to the north and the highlands of the Tibetan Plateau to the south. The basin is known to have been a significant depocenter in Pliocene and Quaternary time (e.g., Craddock et al., 2010), but the early history of basin fill is largely unknown (cf. Zhang et al., 2012). We combine geologic mapping of deformed Tertiary sediments with stratigraphic and sedimentologic observations to place constraints on the relative timing of range growth and sediment accumulation along this margin of the Gonghe Basin. Absolute chronology is established using magnetic reversal stratigraphy, correlated to the geomagnetic polarity time scale through tie points determined from cosmogenic burial ages in alluvial sediment (e.g., Granger et al., 1997). This novel approach to establishing a radiometric basis for magnetic reversal stratigraphy allows us to bracket the onset of deformation along the fault systems bounding the Gonghe Basin.

CENOZOIC TECTONICS OF THE NORTHEASTERN TIBETAN PLATEAU

Early Tertiary Sedimentation in Xining-Lanzhou and Western Qaidam

The northeastern part of the Tibetan Plateau, which is covered by broad sedimentary basins and transected by narrow elongate mountain ranges, has been the site of protracted basin formation since at least the Early Cretaceous. Stratigraphic archives from Xining and Lanzhou Basins (Fig. 1), near the periphery of the northeastern Tibetan Plateau, indicate slow subsidence (~10 m/m.y.) from the Early Cretaceous until the mid–late Tertiary (Horton et al., 2004; Dai et al., 2006). The low rate and broad spatial

extent of sediment accumulation in the Linxia-Lanzhou region likely reflect Cretaceous and Paleogene thermal subsidence following extensional deformation across north China during the latest Jurassic and Early Cretaceous (e.g., Vincent and Allen, 1999; Meng et al., 2003; Horton et al., 2004).

This relatively quiescent regime appears to have been interrupted by deformation in Paleogene time. Paleomagnetic determinations suggest clockwise vertical-axis rotation of the Xining Basin between ca. 45 and 30 Ma (Dupont-Nivet et al., 2004, 2008); bedrock thermochronology suggests enhanced cooling and exhumation along the West Qinling Shan at ca. 45–50 Ma (Clark et al., 2010), which appear to reflect activity along the range-bounding fault (Duvall et al., 2011); and accelerated sedimentation in the Linxia Basin (Fang et al., 2003) at ca. 30 Ma implies increased subsidence at this time. Collectively, these proxy data suggest that the northeastern Tibetan Plateau experienced an episode of tectonism near in time to the initial collision of India with Eurasia (Clark et al., 2010), which most workers attribute to a far-field response to Indo-Asian collision (e.g., Dayem et al., 2009).

Similar geologic evidence exists for deformation in the western Qaidam region, where several broad depocenters began developing in the early Eocene (Yin et al., 2007). Regional patterns of sediment thickness and geologic relationships observed within seismic profiles suggest that the development of early Tertiary depocenters was related to growth of regional thrust belts along the northwestern and southwestern margins of the Qaidam Basin (Yin et al., 2008b; Bovet et al., 2009). Thermochronologic cooling histories in the eastern Kunlun Shan, along the southern margin of the Qaidam Basin, also reveal an increase in exhumation rate at ca. 35–30 Ma (Mock et al., 1999; Clark et al., 2010). Whether tectonism along the western Qaidam Basin was linked with early Tertiary depocenters of the northeastern Tibetan Plateau, however, remains an open question. Thus, one of the goals of this work is to characterize the history of sediment accumulation in one of the primary depocenters between these regions, the Gonghe Basin.

Late Cenozoic Mountain Building

Emerging results from studies around the peripheral regions of the northeastern Tibetan Plateau suggest that much of the present-day topography developed since the middle Cenozoic (e.g., Molnar, 2005, and references therein). Although the Altyn Tagh fault likely had a Mesozoic ancestry (Darby et al., 2005), the sinistral slip that presently characterizes the fault did not initiate until ca. 25 Ma (Yue et al., 2003; Ritts et al., 2008). Subsequently, a sharp decrease in rates of left-lateral slip along the Altyn Tagh fault (Yue et al., 2003; Ritts et al., 2008) and surface uplift of the Altun Shan both occurred around ca. 15–18 Ma (Ritts et al., 2008; Kent-Corson et al., 2009). The southernmost and northernmost thrust systems bounding the Qilian Shan–Nan Shan appear to have been activated at ca. 8–10 Ma (George et al., 2001; Jolivet et al., 2001; Fang et al., 2007; Bovet et al., 2009; Zheng et al., 2010; Zhang et al., 2012). Along the northeastern periphery of the plateau, the Liupan Shan experienced accelerated exhumation at ca. 8–11 Ma (Zheng et al., 2006; Wang et al., 2011), which appears to reflect the onset of shortening associated with the eastern terminus of the Haiyuan fault system (Wang et al., 2011).

The interior northeastern Tibetan Plateau appears to have experienced a similar history. Stratigraphic and thermochronologic data suggest that shortening along the Laji-Jishi Shan corridor (Fig. 1) initiated at ca. 20–22 Ma (Lease et al., 2011, 2012), but it accelerated in the time period between ca. 14 and 8 Ma (Fang et al., 2005; Lease et al., 2007, 2011, 2012; Hough et al., 2011). This latter event is marked by distinct increases in sediment accumulation rate and changes in provenance in the Linxa region (Dettman et al., 2003; Fang et al., 2003; Zheng et al., 2003; Garzione et al., 2005) to the east of the Jishi Shan (Fig. 1). However, the spatial patterns of range growth farther west, in the interior regions of northeastern Tibet (Fig. 1), remain uncertain. An understanding of the degree to which Neogene mountain building was coordinated between the plateau margin and interior will indicate whether mountain building was driven by a fundamental shift in the dynamics of intracontinental deformation (e.g., Molnar, 2005), or whether mountain building reflects a progressive thickening of crust (e.g., Clark and Royden, 2000; Tapponnier et al., 2001).

Evolution of the Gonghe Basin Complex

To address these questions, we conducted an investigation of Tertiary stratigraphy along the southern margin of the Gonghe Basin. The greater Gonghe Basin complex covers a broad, ~200 × 200 km region, the northern and southern portions of which are associated with the Qinghai Nan Shan and the Gonghe Nan Shan, respectively (Fig. 1). Both ranges are ESE-striking, extend over hundreds of kilometers, and are developed above active, south-vergent thrust systems. Ranges along strike from the Qinghai Nan Shan to both the east and west, in the southern Qilian Shan and Laji Shan, respectively (Fig. 1), exhibit evidence for thrust faulting in Neogene time (e.g., Fang et al., 2005, 2007; Lease et al., 2007, 2011, 2012). South of the basin, there is the Anyemaqen Shan, a broad region of high elevation that marks a step from elevations of 4500–4000 m on the plateau to the south to the ~3500 m elevations of the Gonghe Basin. Although the precise timing for development of this relief remains uncertain, analysis of river profiles (Harkins et al., 2007) and the presence of active faults within the range (Harkins et al., 2010) suggest that it is relatively young.

The Gonghe Basin complex is an amalgamation of several depocenters, which are referred to here as the Gonghe, Tongde, and Chaka subbasins (Fig. 2). Each of these contains strata deposited unconformably atop a basement of complexly deformed Triassic rocks (Fig. 1). Despite the potential tectonic significance of these sedimentary archives, constraints on the age of sedimentary deposits in the Gonghe (sensu lato) region are few, and, until recently, age constraints were derived almost entirely from regional lithostratigraphic correlation (e.g., QBGMR, 1991). In Gonghe and Tongde subbasins, the fill is capped by an ~300–600 m succession of alluvial gravels, sands, and muds (Zheng et al., 1985; Craddock et al., 2010). A combination of paleontologic markers, magnetostratigraphy, and cosmogenic burial ages suggests that these strata accumulated in Tongde from ca. 3.4 to 0.5 Ma (Craddock et al., 2010). Sparse biostratigraphy in the central Gonghe Basin suggests a similar history (Zheng et al., 1985), but to date, absolute age constraints for the upper part of southern Gonghe Basin fill are unavailable. For the deeper levels of basin fill in southern Gonghe and central Tongde, age constraints and stratigraphic information are entirely lacking.

A recent stratigraphic study along the northwestern margin of the Chaka subbasin provided the first indication that sediment accumulation began prior to the Pliocene (Zhang et al., 2012). Chaka subbasin is floored by ~700 m of muddy, fluvial and lacustrine deposits that date to ca. 12–8.6 Ma (Zhang et al., 2012). Overlying the basal deposits, there is an 800-m-thick package of fluvial deposits, which coarsens upward into a >300-m-thick package of alluvial-fan deposits. The two packages of sediment date to 8.6–4.6 Ma and 4.6–<3.0 Ma, respectively (Zhang et al., 2012), and they are interpreted to indicate that growth of the Qinghai Nan Shan initiated locally at ca. 6 Ma (Zhang et al., 2012).

In Tongde Basin, a combination of cosmogenic burial ages for the uppermost basin fill and dating of strath terraces along the Yellow River reveals a transition from basin filling to excavation in greater Gonghe at ca. 0.5 Ma (Craddock et al., 2010). This transition has been linked to a

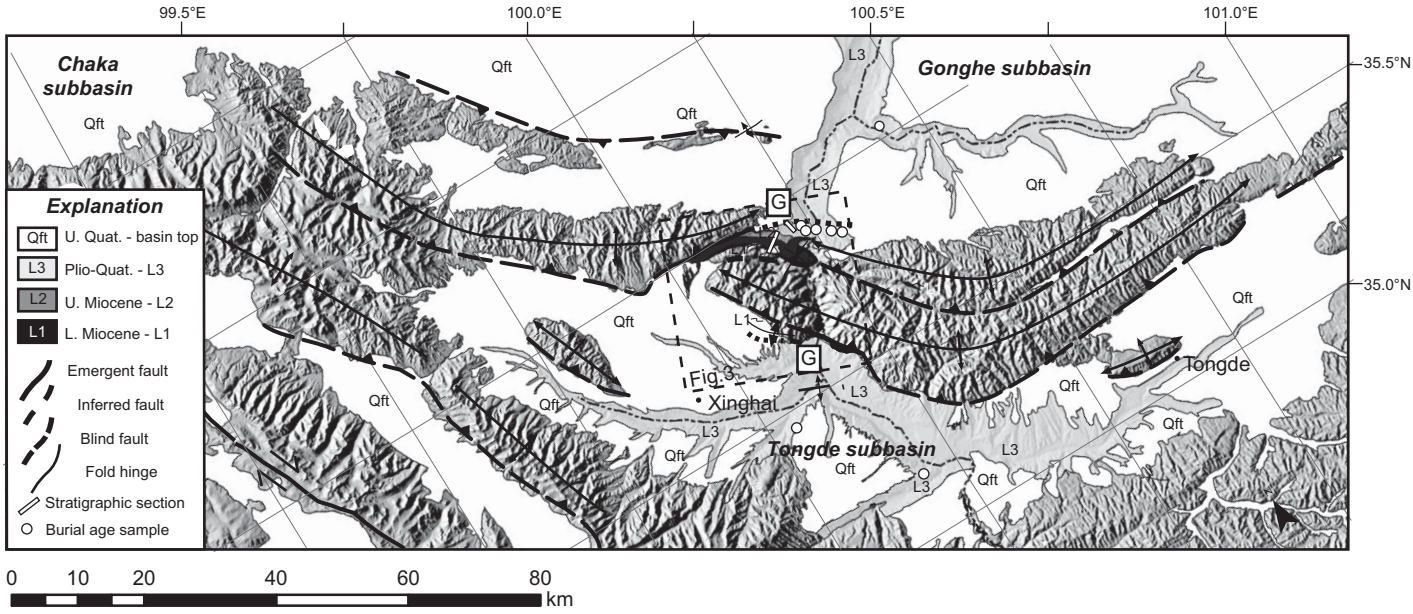

Figure 2. Geology of the southern Gonghe Basin complex. White bars show location of measured sections. White circles show burial age sites, and the samples in Tongde subbasin are from Craddock et al. (2010). Sites labeled G exhibit progressive unconformities and growth strata. Cross section A-A′ (Fig. 4) is NNE-striking and contained within the central part of the box that defines the location of Figure 3.

regional episode of headward erosion along the Yellow River, perhaps related to the spillover of a lake from a closed basin near the plateau margin in the earliest Pleistocene (Harkins et al., 2007; Craddock et al., 2010). A recent terrace chronology from central Gonghe suggests that basin excavation may be slightly more recent than previously envisaged; cosmogenic dating of surface clasts atop the highest strath terrace in the region are interpreted to constrain terrace abandonment at ca. 125–250 ka (e.g., Perrineau et al., 2011). However, multiple unconformities within the terrace deposits and a poorly constrained history of loess accumulation and stripping suggest that this age is almost certainly a lower bound. Regardless, an absolute chronology for the uppermost levels of basin fill in the central Gonghe Basin would help to better resolve the precise timing of incision in the Gonghe Basin (sensu stricto) and the evolution of the Yellow River across northeastern Tibet.

STRUCTURAL GEOLOGY OF THE GONGHE NAN SHAN

To better constrain the geometry of folds and fault systems associated with the Gonghe Nan Shan, we augmented existing 1:200,000 geologic maps (QBGMR, 1991) with detailed, 1:24,000 scale mapping at key sites along basin margins where strata range from slightly to highly deformed (Figs. 2 and 3) and with reconnaissance-level observations in the relatively undeformed center of the basin. Overall, the exposures of basin strata on both the northern and southern sides of the Gonghe Nan Shan reveal that the range is cored by a broad asymmetric anticline, associated with an underlying network of south-vergent imbricate thrust faults. The interior of the range is composed of Triassic flysch deposits that are inferred to form the floor of the basin. To the north and south of the Gonghe Nan Shan, ~500-m-deep exposures of basin fill within the Yellow River canyon reveal subhorizontal, undeformed strata, suggesting that deformation is localized along the basin margins.

In the canyon on the southern side of the range, the range-bounding fault outcrops and dips ~30° to the north (Figs. 3 and 4). Patchy exposures of red beds rest unconformably against the southern range front and range from subvertical to overturned, in places dipping back to the northeast (Figs. 2, 3, and 4). Beds within these outcrops can be traced along strike of the range front into discontinuous patches of black and gray sandstones and mudstone. Immediately adjacent to the southern range front, the overlying succession of Cenozoic basin strata exhibits bedding dips that progressively decrease up section (Figs. 3 and 4), and the uppermost alluvial gravels that cap the basin are subhorizontal. These geometries suggest significant slip along the range front fault system during deposition of basin strata.

In the canyon on the north side of the range, mapping along multiple structural transects indicates that basal portions of Gonghe Basin strata are exposed along a 20–30°NNE dip panel that parallels the northern flank of the range (Figs. 3 and 4). Overlying strata onlap a low-relief surface that is preserved along the northern flank of the Gonghe Nan Shan (Figs. 2 and 3); this surface dips ~30°N and appears to represent an extensive low-relief surface similar to that observed on the plateau to the south and east (Clark et al., 2010; Harkins et al., 2007). Bedding dips along the northern range flank also progressively decrease up section, such that dips in the thick succession of alluvial gravels that caps the basin exhibit a fanning pattern, ranging from 0° to 15°.

Tertiary strata can be traced over the crest of the range along a broad canyon that runs between two local villages, Jiala and Yangqu (Fig. 3). Map patterns close to the northwest, reflecting a gently plunging anticlinal axis (Fig. 3). This structure is truncated to the north by another south-vergent thrust fault that carries Triassic rocks over the folded Tertiary strata (Fig. 3). South and east of the village of Yangqu (Fig. 3), deformed strata define the western tip of another NW-plunging anticline. The trace of this secondary fold coincides with a prominent topographic break in the central Gonghe Nan Shan, and remnants of Cenozoic foreland basin strata are preserved in the structural and topographic saddle in the middle of the range (QBGMR, 1991) (Fig. 2). Thus, there appears to be a third major thrust fault that juxtaposes

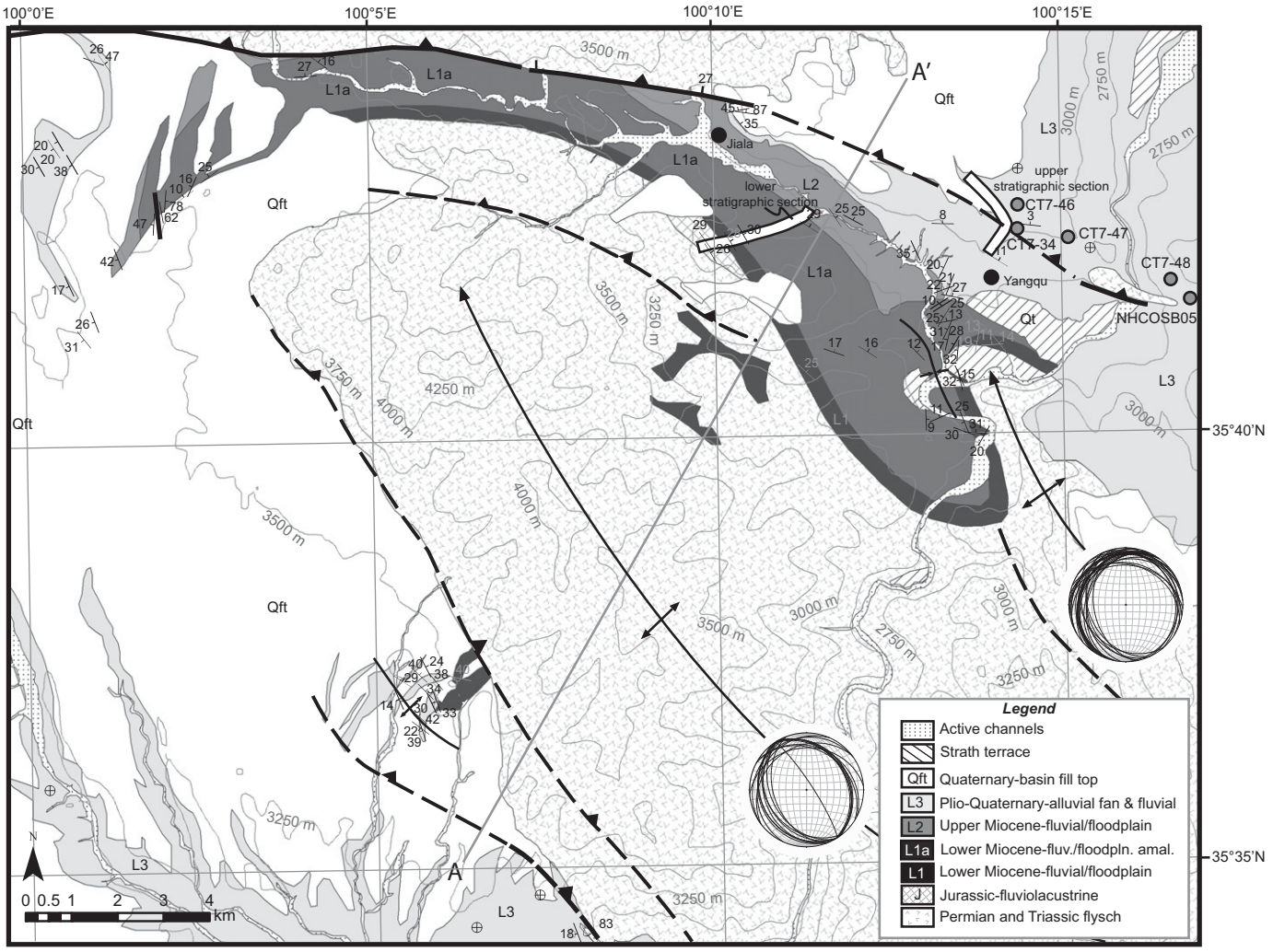

Figure 3. Detailed map of the central Gonghe Nan Shan in the Yellow River canyon area.

panels of Triassic strata within the Gonghe Nan Shan. Overall, the structures appear to represent a south-vergent imbricate fan of faults that roots northward beneath the Gonghe Basin.

CENOZOIC BASIN STRATIGRAPHY

In order to characterize the stratigraphic architecture of the basin, we measured a 1350 m section that spans the Cenozoic basin fill (Fig. 5). The section was measured in a network of deep canyons on the northern flank of the range (Figs. 2 and 3), and it is a composite of a lower section that extends to the basin floor and an upper section that extends to the top of the Gonghe Basin fill. A small river valley and an adjoining small alluvial-fan complex cover the top of the lower section, and along much of this valley, the upper section rests unconformably on strata associated with the lower one. We estimate that an ~150 m section of basin fill is covered across this small valley on the basis of (1) measured stratigraphic thickness in the field and (2) the plan-view width of the valley and the bedding dip of adjacent strata. Although it is difficult to evaluate the thickness that is truncated across the unconformable contact between the sections, regional geologic relationships suggest that it is small. Specifically, beds dip almost concordantly across the contact, whereas, at structurally high positions near the basin floor, the angular unconformity is nearly 30°. Given the progressive rotation of beds in the proximity of this contact, we infer the diminished angular unconformity to reflect relatively complete stratigraphic preservation, with no more than several tens of meters of truncated section. Several distinctive lithofacies are present in southern Gonghe (Table 1), and assemblages of these facies define three lithostratigraphic units (Table 2). In the following section, we describe the stratigraphy of the southern Gonghe stratigraphic section. In an effort to link the strata to the evolution of the Gonghe Nan Shan, we also present paleocurrent measurements and conglomerate clast descriptions from key stratigraphic intervals. Field photos of each stratigraphic unit are provided in GSA Data Repository section 1.[1]

At the base of the lower section, an ~200-m-thick accumulation of lithostratigraphically distinctive sediments that bear Jurassic–Cretaceous pollen sits unconformably below our measured section. Detailed stratigraphic observations and Jurassic–Cretaceous pollen

[1]GSA Data Repository Item 2011351, supplementary stratigraphic, cosmogenic burial age dating, and paleomagnetic information, is available at www.geosociety.org/pubs/ft2011.htm, or on request from editing@geosociety.org, Documents Secretary, GSA, P.O. Box 9140, Boulder, CO 80301-9140, USA.

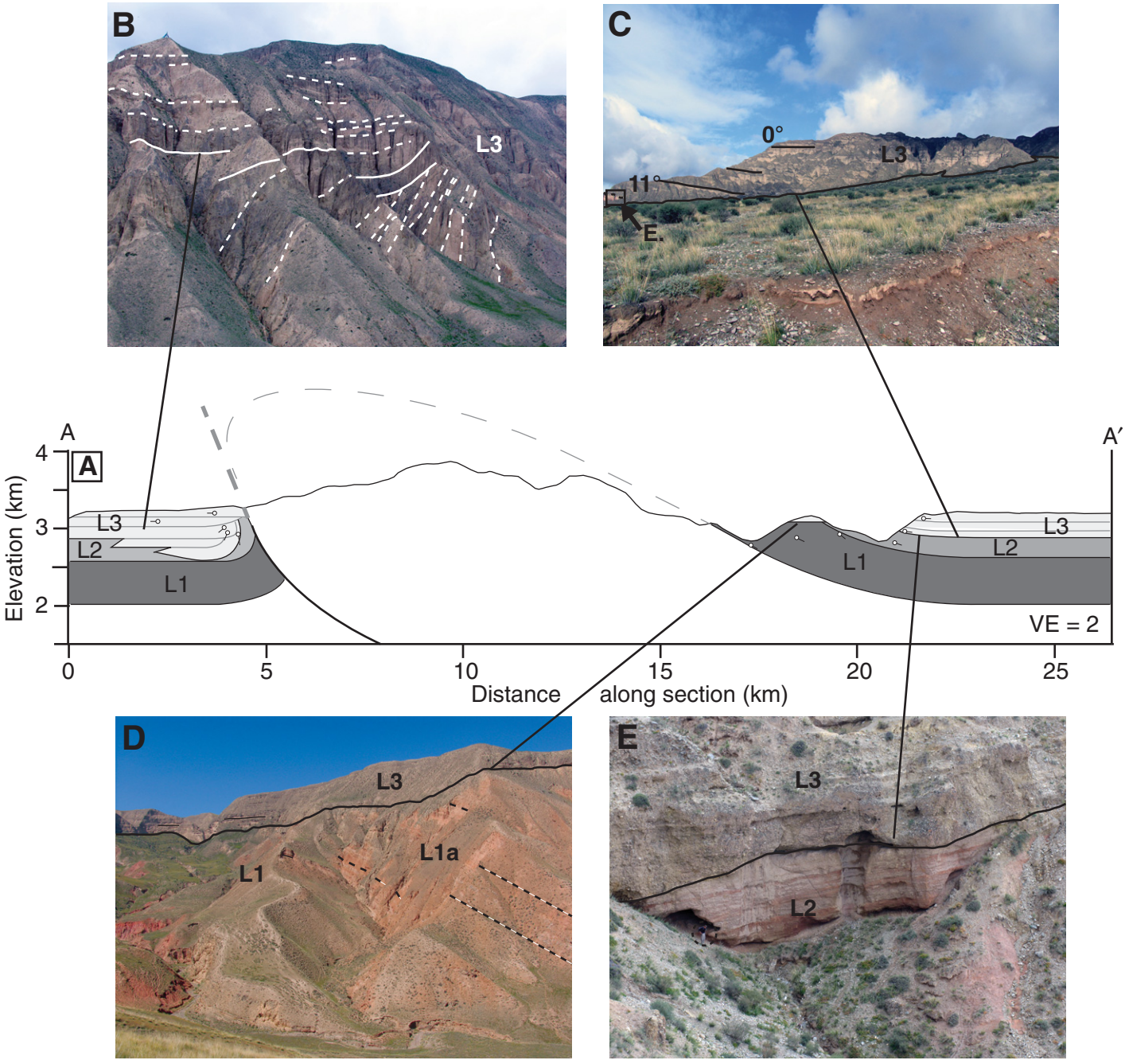

Figure 4. (A) Simplified geologic cross section and supporting photographs showing relationships between basin strata and faults. Location of cross section is shown on Figure 3. (B) Growth strata and progressive unconformity on the southern flank of the Gonghe Nan Shan in the Yellow River canyon. Cliff is ~200 m high. (C) Growth strata on the northern flank of the Gonghe Nan Shan, in the Yellow River canyon. Cliff is ~300 m high. (D–E) Progressive unconformity on the northern flank of the Gonghe Nan Shan near the Yellow River canyon. C is located near the base of the lower stratigraphic section in southern Gonghe, whereas D is located at the base of the upper stratigraphic section, such that the unconformity between L3 and underlying rocks diminishes away from the Gonghe Nan Shan. The cliff in D is ~300 m high. The geologist circled in E is ~2 m tall. VE—Vertical exaggeration.

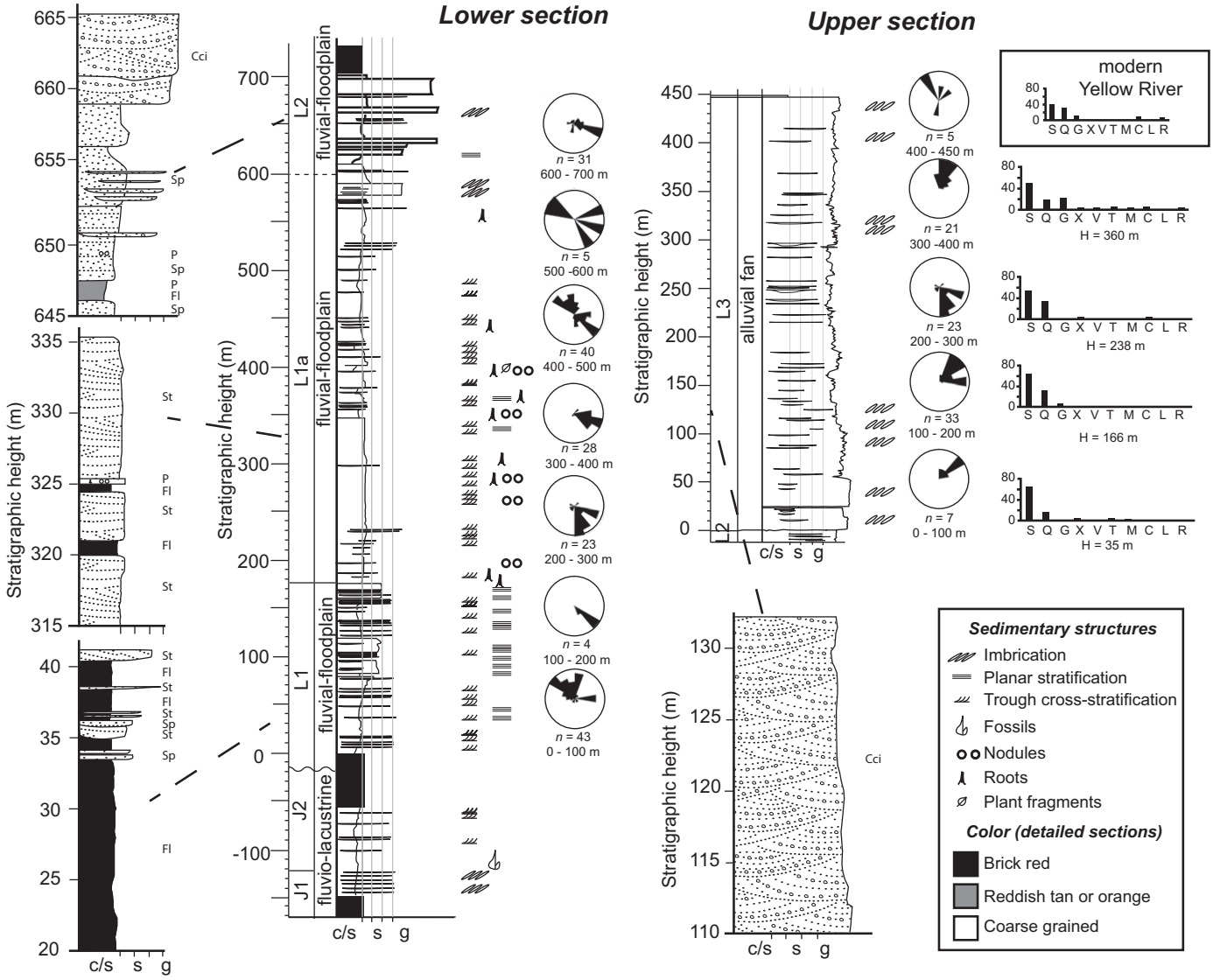

Figure 5. Lithostratigraphy, paleocurrents, and clast composition of lower and upper stratigraphic sections in southern Gonghe. In rose diagrams, the radius is equal to the number of measurements in the largest bin. The petal width is 20°. S—sandstone, Q—quartz, G—granite, X—no clast, V—volcanics, T—schist, M—marble, C—matrix-supported conglomerate with green or red matrix and rounded clasts, L—shale, R—chert. Locations of sections are shown in Figures 2 and 3. c/s—clay and silt, s—sand, g—gravel.

TABLE 1. LITHOFACIES AND INTERPRETATIONS

Code	Facies	Structures	Interpretation
Fl	Sandstone, siltstone, mudstone	Massive or fine lamination	Overbank or waning flood deposits
P	Paleosol, calcite-cemented sandstone or mudstone	Pedogenic features	Soil formation on floodplain
Sr	Very fine- to coarse-grained sandstone	Ripple cross-lamination	Ripples (lower-flow regime)
St	Very fine- to coarse-grained sandstone	Solitary or grouped trough cross-beds	Sinuously crested and linguoid 3-D dunes
Sp	Very fine to fine sandstone	Massive or fine lamination	Rapid sedimentation, upper plane bed
Cci	Conglomerate, stratified, clast supported	Imbrication	Longitudinal bed forms, lag deposits

Note: Adapted from Miall (2000).

TABLE 2. LITHOSTRATIGRAPHIC UNITS

Lithostratigraphic unit	Major facies codes	Minor facies codes
Lithostratigraphic unit 1	Fl, St, Sp	P, Sr
Lithostratigraphic unit 1a	St, Sp	Fl, P, Sr
Lithostratigraphic unit 2	St, Sp, Cci	Fl, P, Sr
Lithostratigraphic unit 3	Cci	N.A.

Note: See Table 1 for definitions of facies codes.

assemblages are presented in Data Repository section 2 (see footnote 1).

Distribution, Description, and Interpretation of Lithofacies Assemblages

Lithostratigraphic Unit 1 (L1)—Lenticular, Trough Cross-Bedded Siltstone and Sandstone Interbedded with Brick-Red Mudstone

L1 is found in the southern part of the Gonghe Basin complex, where it is folded over the Gonghe Nan Shan. It is ~600 m thick. It is also found in discontinuous patches along the southern flank of the range (Fig. 2). L1 consists of tabular intervals of brick-red mud interbedded with lenses of sandstone and siltstone (Fig. 5). Coarser-grained beds exhibit sharp basal contacts that tend to be gently curved, with relief of up to a few tens of centimeters. Channel scours are found along the bases of these beds. The relatively coarse beds exhibit trough cross-bedding with troughs 10–30 cm deep and horizontal lamination, and they commonly exhibit pebble lags. The coarser beds range from 0.1 to 1.5 m thick, and they are continuous over tens to hundreds of meters. They typically comprise multistory channel complexes that are a few meters thick and contain 3–10 lenticular beds of siltstone to coarse sandstone. These channel complexes are generally separated by a 1–3 m of mudstone. Mudstone beds are commonly massive tabular sheets that occasionally exhibit planar parallel lamination. Mudstones commonly show gray and orange mottling, often along laminae surfaces. Muddy intervals contain carbonate nodules and concretions, burrows, and roots, and they exhibit a prismatic texture. The muds contain abundant red, gray, and white, laterally continuous, ~1–5-cm-thick calcite-cemented bands. Red and white bands are also found in massive and cross-bedded sandstone beds. A variation of L1, which we dub L1a, is identical to L1 except that it is dominated by amalgamated siltstone and sandstone beds that are up to tens of meters thick with thin mud interbeds or parting (Fig. 4).

We interpret the sandy, cross-bedded lenses of sand to represent channel deposits. The sets of trough cross strata are interpreted to represent migrating, three-dimensional dunes deposited under unidirectional, lower-flow regime transport conditions (Harms et al., 1982). Planar parallel-laminated beds suggests that some beds were deposited under unidirectional, upper-flow regime transport conditions (Harms et al., 1982), although some may be deposits from the waning stages of floods (Collinson, 1996). The lenticular geometry, as well as the scours along the base of some beds, indicates that the flow was channelized. The coarse grain size and lack of small-scale cross-bedding or ripples suggest that these are not levee deposits (Singh, 1972; Collinson, 1996), although some may represent splay deposits emanating from deeply incised crevasses (Collinson, 1996). We interpret the finer beds to represent overbank deposits. The grain size and massive bedding of these deposits indicate that the sediments settled out of suspension. The carbonate nodules, concretions, and calcite-cemented bands are likely the result of illuviation on a floodplain (Collinson, 1996). The prismatic texture, roots, burrows, and deep-red oxidation of the fine-grained beds likely reflect pedogenesis during prolonged periods of subaerial exposure (Collinson, 1996; Miall, 1996).

Lithostratigraphic Unit 2 (L2)—Horizontally Laminated Orange and Tan Sheet-Like Siltstone Interbedded with Gray Conglomerate and Multicolored Mudstone

L2 is found extensively across the southern Gonghe Basin complex. At our measured section, it is ~250 m thick before it is covered in the river valley at the top of our lower section. Correlative L2 outcrops appear in the base of deep canyons in central Tongde (Craddock et al., 2010). The unit consists of light red-orange or buff-colored, very fine- to coarse-grained sandstone (Fig. 5). Finer parallel-laminated sandstones and mudstones appear to be tabular at the scale of an outcrop, but they pinch out laterally, over length scales of hundreds of meters. These beds are interbedded with 1–3-m-thick, laterally continuous, clast-supported conglomerates, or trough cross-bedded or planar parallel-laminated medium to coarse sandstone. Conglomerate beds exhibit irregular basal contacts, with, at most, a few tens of centimeters of relief. The conglomerate clasts are imbricated, and the beds exhibit tabular geometry. Clasts are poorly sorted and subrounded to angular. The unit is also interbedded with tabular bands of gray, and brownish- and greenish-gray massive mudstone and siltstone. Red and white, ~1–5-cm-thick, calcite-cemented bands are often present in this unit.

Similar to L1, we interpret the abundance of indicators for unidirectional flow and paleosol development to indicate deposition in a fluvial-floodplain environment (e.g., Collinson, 1996; Miall, 1996). L2 differs from L1 on the basis of (1) the relatively low degree of oxidation in L2 indicated by the orange color of the mudstones, (2) the presence of meter-thick conglomerate bands, and (3) the more tabular, versus lenticular, geometry of the beds. The silty, planar parallel-laminated, tabular beds that comprise most of L2 may represent crevasse splays (Collinson, 1996), and may reflect increased abundance of overbank deposits in L2 in comparison to L1.

Lithostratigraphic Unit 3 (L3)—Imbricated Conglomerate

L3 caps the Gonghe Basin complex, and along the southern margin of Gonghe, it is ~450 m thick (Figs. 2 and 5). L3 strata can be traced to the south through a structural saddle in the Gonghe Nan Shan and into Tongde Basin, such that the upper basin fill in southern Gonghe is correlative to the uppermost strata in Tongde. In the northern Tongde Basin, L3 is ~400–500 m thick, and these strata can be traced south along the wall of the Yellow River canyon for tens of kilometers. L3 strata interfinger toward the south with sandier deposits, and they are directly correlative with the Pliocene–Quaternary fluvial sands and gravels in central Tongde Basin (Craddock et al., 2010). The unit is composed of pebble or cobble, clast-supported conglomerate with a buff-colored muddy matrix and with buff, sandy and silty lenses (Fig. 5). The bedding is lenticular and laterally continuous over single digits to hundreds of meters. Beds are tens of centimeters to a few meters thick. Clast sizes range from 20 to 200 mm. The clasts are unsorted to poorly sorted, and subangular to subrounded. Sand lenses are separated by a few meters, they exhibit decimeter-scale thickness, and they are a few meters to tens of meters wide. Sedimentary structures include imbrication, channel scours, large (10–100 cm high) cross-bedding within gravel beds, and parallel- or cross-lamination in finer lenses.

This facies assemblage is interpreted to represent braided channel alluvial-fan deposits. Imbricated, cross-bedded, and parallel-planar beds indicate traction deposition in a unidirectional flow (Harms et al., 1982; Nemec and Postma, 1993). The lenticular geometry of the beds and the channel scours along the base of the beds indicate the presence of discrete channels. The distribution of L3 along the Gonghe Nan Shan range front suggests that it is an alluvial-fan deposit, rather than the thread of a gravel bed-load dominated river. The absence of (1) matrix support, (2) inverse grading, and (3) tabular geometry distinguishes these beds from debris-flow–dominated alluvial-fan deposits (Nemec and Steel, 1984).

Paleocurrent Analysis

Paleocurrent indicators were measured along stratigraphic sections in southern Gonghe and Tongde (Fig. 5). We sought unidirectional paleocurrent indicators, particularly trough cross-bedding and imbricated conglomerate clasts (Tucker, 2003), and obtained 20–40 individual measurements at most sites. Because three-dimensional exposure was limited in many outcrops, we ascribe an uncertainty to our measurements of ±30°. Although measurements from

the lower Gonghe section were taken from tilted beds, leading to slight differences between our measurements and the true paleoflow direction, the shallow dip of the beds (<30°) means that the maximum postdepositional deflection is ~15° (assuming simple unfolding along a horizontal axis). This error is well within the uncertainty we ascribe to our measurements and is not sufficient to bias first-order paleocurrent patterns that we observe.

In L1, paleoflow directions are dominantly ~ESE in the lower ~400 m of the stratigraphic section (Fig. 5). Between 400 and 600 m, paleocurrents were either ESE or WNW, but above 600 m, paleocurrent directions return to ESE in L1 and L2. In contrast, however, paleocurrent determinations in unit L3 suggest flow toward the NNE (Fig. 5). This ~90° shift in paleoflow direction between the lower and upper sections is significant, even within the uncertainties on our data.

Clast Provenance

We conducted clast counts at four different sites within L3 in southern Gonghe, and within the tread of one modern Yellow River terrace (Fig. 5). At each site, we counted ~100 clasts. In general, the clast composition of L3 is fairly monotonous; most sites are dominated by sandstone and quartz. Two sites exhibit a much more diverse assemblage of clasts compared to the others. The first is the terrace tread along the Yellow River near Gonghe city. The second is the highest measurement site from intact fill in southern Gonghe, ~100 m below the top of the basin (at 358 m). The sites contain a lower overall percentage of sandstone and quartz, and they contain a high percentage of granite (compared to a few percent granite at other sites), as well as a variety of rocks such as volcanic rocks and green and red matrix-supported pebble conglomerates with well-rounded clasts. The southern Gonghe site marks the base of a pronounced transition in the clast composition of L3. Below this horizon, clast composition is similar to other L3 outcrops around southern Gonghe and Tongde. Above this horizon, however, the clast assemblage becomes much more diverse, and the clasts consists of a higher percentage of granite as well as significant amounts of other rock types.

EVIDENCE FOR SYNTECTONIC SEDIMENTATION

Sedimentologic Evidence

The entire stratigraphic package in southern Gonghe coarsens upward, suggesting the development of high topography adjacent to southern Gonghe during basin filling (Fig. 5). In particular, the onset of alluvial-fan sedimentation, along both the northern and southern flanks of the range, appears to be directly linked to the emergence of a high-relief source region. Moreover, the corresponding shift to NNE paleocurrents at the onset of L3 deposition suggests that sedimentation occurred in the shadow of a topographic high to the south. The ESE-oriented paleocurrents in L1 and L2 derive from a structurally high position on the northern flank of the Gonghe Nan Shan. Implied transport directions are highly oblique to the present-day topography, suggesting that range growth postdates deposition of these strata.

The provenance of conglomerate clasts in L3 is also consistent with syntectonic deposition. Lower strata within L3 are dominated by sandstone and quartz, which are common to the Triassic flysch that constitutes the core of the Gonghe Nan Shan. Importantly, the Triassic rocks are regionally ubiquitous (e.g., QBGMR, 1991), such that their presence in L3 strata does not uniquely link the deposits to the range. The appearance of a diverse assemblage of clasts, which mirrors the composition of Yellow River terrace lags, suggests that an exotic sediment source was also involved in basin filling, and suggests that the upper Yellow River predates the development of the Gonghe Nan Shan (a point also argued by Craddock et al. [2010] on the basis of continuity of the basin fill surface across the range).

Growth Strata

Progressive unconformities and growth strata are present along both the southern and northern flanks of the Gonghe Nan Shan, and they unequivocally link L3 sedimentation to range growth (Fig. 4). In the Yellow River canyon on the southern side of the range, L3 conglomerate beds are in unconformable contact with the highly deformed metasedimentary rocks that form the core of the interior of the range. Within this canyon wall, dips of L3 strata decrease progressively up section along the ~150-m-high canyon wall; the beds are subvertical just above the basal unconformity, and they are subhorizontal at the basin surface (Fig. 4B). Moreover, in this outcrop, L3 exhibits prominent intraformational unconformities in which tilted strata are truncated by relatively flat-lying, overlying strata. These unconformities can be traced into correlative conformities only a few hundred meters to the south. On the northern side of the range near the village of Yangqu, a 450-m-thick exposure of L3 gravels crops out on the western Yellow River canyon wall. Bedding dips in this outcrop also progressively decrease up section in this canyon wall; they dip 11°NE at the base of canyon and 0° at the top (Fig. 4C). This package of strata with fanning dips corresponds to the section of L3 strata that exhibit a pronounced stratigraphic transition to alluvial-fan deposition and an ~90° paleocurrent shift. Furthermore, at several outcrops in this area, L3 is in angular unconformable contact with underlying L1 and L2 deposits, and the unconformity diminishes moving away from the Gonghe Nan Shan (Figs. 4D and 4E).

CHRONOLOGY OF STRATIGRAPHIC UNITS

Sample Scheme for Dating Stratigraphic Units

In order to place absolute constraints on the age of the deposits in southern Gonghe, we developed a chronology that is based on both absolute ages from the decay of the cosmogenic isotopes ^{26}Al and ^{10}Be (e.g., Granger, 2006) and correlation of magnetic polarity stratigraphy to the geomagnetic polarity time scale (GPTS) (Ogg and Smith, 2004). For burial age dating, six new samples of coarse fluvial sand were collected from L3 exposures from the base of modern road cuts (Fig. A2 [see footnote 1]), where we are able to constrain sample depth prior to historic road construction. Samples were collected at sites from 82 to 317 m below the top of the basin fill (supplementary information section 3 [see footnote 1]). Four of the samples were collected within a few kilometers of the upper stratigraphic section and are readily correlated into syntectonic L3 strata along the southern Gonghe stratigraphic section. Moreover, these samples are regionally correlated to dated L3 strata in the Tongde subbasin (Craddock et al., 2010). A fifth sample was gathered from a 5-m-deep cave within the upper southern Gonghe stratigraphic section. A sixth sample, however, was collected from the south-central Gonghe Basin, ~20 km to the northeast of the measured section along the Gonghe Nan Shan (Fig. 2; Table 3), and its position in the stratigraphic section is considered approximate. In general, we selected samples that were buried by ~15–30 m of sediment prior to road construction, i.e., sufficiently deep such that postburial muogenic production is minimal (Granger and Muzikar, 2001).

We collected magnetostratigraphic samples along both stratigraphic sections in southern Gonghe Basin (Figs. 2 and 3). The two sections were selected because they offer relatively continuous exposure of key stratigraphic intervals of the Gonghe Basin fill, and the sections were structurally relatively simple. As is typical of many stratigraphic and magnetostratigraphic studies, the sections represent composites of

TABLE 3. BURIAL AGE SAMPLE INFORMATION

Sample number	Location		Elevation (m)	Depth (m)	[^{10}Be] (atoms/g$_{quartz}$)	1σ uncertainty (atoms/g$_{quartz}$)	[^{26}Al] (atoms/g$_{quartz}$)	1σ uncertainty (atoms/g$_{quartz}$)
	Lat. (°N)	Long. (°E)						
CT7-11	35.77042	100.43448	2839	301	67,604	3945	75,976	15,928
CT7-34	35.70796	100.23941	3043	101	104,310	5641	221,142	46,421
CT7-46	35.71263	100.23899	3130	82	220,310	7655	1,158,031	98,315
CT7-47	35.70605	100.25145	3025	187	18,433	3429	31,534	19,672
CT7-48	35.69759	100.27609	2938	271	8126	1290	8849	5903
NHCOSB0	35.69378	100.28083	2892	310	174,000	7000	41,000	36,000

several shorter sections. We correlated subsections in the field, typically over distances on the order of ~100 m, and we measured and sampled overlapping stratigraphic intervals for all of the subsections. We sought to collect samples at 2–5 m intervals, in order to obtain a high-resolution magnetostratigraphy. At each sample site, we collected 3–5 specimens. Most specimens were collected in situ as 2.5-cm-diameter core using a gas-powered drill, and in general, we sought to sample mudstones and siltstones. The lack of mudstones in the upper basin fill occasionally required the sampling of relatively friable fine and medium sandstones. Occasionally, sandstones were too friable to sample by drill, and in these instances, we collected oriented block samples, ~125 cm^3 in volume. For the lower section, our average sample spacing was 3.1 m. The upper section consists almost entirely of conglomerate (Fig. 5), and we exploited sandstone lenses for sampling. The spacing of these sandstone lenses limited our sample spacing to 11.2 m. The upper ~40 m of section were impossible to sample because of a lack of sandstone lenses, meaning that our magnetostratigraphy does not extend to the highest levels of Gonghe Basin fill. Given average sedimentation rates from the Tongde Basin of ~50–100 m/m.y. (e.g., Craddock et al., 2010), our sample spacing suggests that ~10–30 k.y. of time separate each sample in the lower section, and 50–100 k.y. separate each sample in the upper section. This level of resolution should be sufficient to facilitate robust identification of magnetic polarity zones, which typically span a few hundred thousands of years in the Cenozoic (Lowrie and Kent, 2004).

Analytical Methods

For burial age determinations, quartz from these samples was isolated and purified using physical and chemical techniques at the Purdue Rare Isotopes Measurement (PRIME) laboratory, following standard procedures. Extraction of ^{10}Be and ^{26}Al was accomplished using cation-exchange chemistry, and the resultant isotope concentrations were measured on the accelerator mass spectrometer at PRIME, following standard protocols (see Data Repository section 3 for a complete description of laboratory methods [see footnote 1]).

For paleomagnetic samples, we implemented a magnetic and thermal cleaning regimen involving a combination of 5–6 alternating field (AF) steps, between 0–100 or 120 gauss, and 14 thermal (TT) demagnetization steps, with a high density below the unblocking temperatures of magnetite and hematite. This regimen is described in detail in Data Repository section 4 (see footnote 1). Cleaning was typically performed on one specimen from each sample site. For 20 sites that exhibited low unblocking temperatures (~350 °C), we conducted cleaning on duplicate specimens, using a higher density of steps, in order to assess the quality of our polarity determinations. Low-coercivity/temperature-component and high-temperature-component magnetization directions were determined using a least-squares fit, principal component analysis (Kirschvink, 1980; Jones, 2002). Additionally, we conducted a range of rock magnetic experiments, including isothermal remnant magnetization (IRM) acquisition, IRM backfield demagnetization, and anhysteric remnant magnetization (ARM) acquisition routines, on a subset of 19 samples in an effort to understand the magnetic mineralogy of the samples. Single-site polarity reversals are retained in our magnetostratigraphy because (1) only specimens with interpretable demagnetization behavior were included in our magnetostratigraphy, (2) certain coarse-grained stratigraphic intervals in the upper section permitted only sparse sampling, necessitating the inclusion of all possible sites, and (3) regional lithostratigraphic considerations suggest that the section is likely to correlate to a portion of the GPTS with relatively short polarity chrons and subchrons (e.g., Ogg and Smith, 2004; Fang et al., 2005; Zhang et al., 2012).

Burial Age Determinations

For buried sediment that is derived from a steadily eroding source, the concentrations of ^{26}Al and ^{10}Be will evolve through time as a function of two unknown variables, the preburial cosmogenic inventory and the time since burial (Granger and Muzikar, 2001; Granger, 2006). We modeled all reasonable combinations of preburial cosmogenic inventory and burial time and used a least-squares optimization to determine a best-fit burial age. We assumed that samples were instantaneously buried to their stratigraphic depth below the basin fill top. Due to the fact that basin excavation appears to be recent and gradual, initiating at ca. 0.5 Ma, or perhaps slightly later, and proceeding at vertical incision rates of ~100 m/m.y. (Craddock et al., 2010; Perrineau et al., 2011), we made the simplifying assumption that postexcavation muogenic production along the evolving hillslope has not contributed significantly to measured cosmogenic inventories (cf. Davis et al., 2011). Recent application of burial age dating to correlative L3 deposits in central Tongde Basin showed that muogenic production following basin excavation by the Yellow River at 0.5 Ma could, at maximum, increase observed burial ages by ~30%, but only under conditions of instantaneous basin excavation and shallowly buried (~15 m) samples (Craddock et al., 2010). For samples buried more deeply, and for slower rates of downcutting along the Yellow River, postburial muogenic production will be significantly less. In light of this sensitivity analysis, we estimate that our calculated burial ages are subject to ~15% uncertainty, which is within the analytical uncertainty of the calculations.

Burial Age Results

We report the observed burial ages and 1σ uncertainties for each of the samples derived from L3 strata. We begin with the shallowest, youngest sample, and move progressively down section (Fig. 6). Overall, the ages are in remarkable stratigraphic order, from about ca. 0.5 Ma at the top of the section to >5 Ma in the lower part of L3 (Fig. A4 [see footnote 1]). CT7-46 was the highest sample, and it was collected in a 32-m-deep road cut, at 82 m below the modern basin fill top (see Figs. A2 and A3). The sample

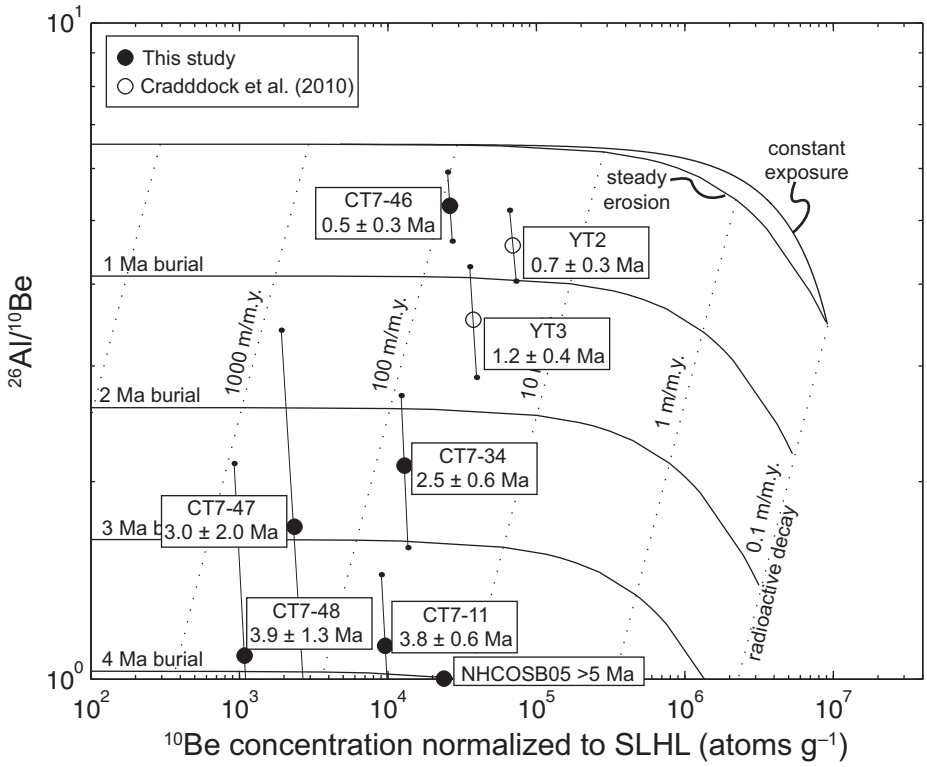

Figure 6. Exposure-burial diagrams and burial ages adjacent to upper southern Gonghe stratigraphic section. Reported 1σ uncertainties represent an average of upper and lower bounds on burial ages/erosion rates. Discrepancy between burial duration contours and calculated burial ages results from postburial in-growth of cosmogenic isotopes because of muogenic production. SLHL—sea level, high latitude.

yields a best fit age of 0.5 ± 0.3 Ma. The age is consistent with recent magnetostratigraphy, biostratigraphy, and cosmogenic burial dating in central Tongde Basin, which shows that basin filling persisted until ca. 0.5 Ma (Craddock et al., 2010). Only ~19 m stratigraphically below the upper sample, sample CT7-34 was collected from a small cave located along the L3 stratigraphic section in southern Gonghe (Fig. A2 [see footnote 1]). The sample was shielded by only ~5 m of material prior to collection, and it yields a significantly older burial age, of ca. 2.5 ± 0.6 Ma. Progressively deeper samples were all collected from 18–36-m-deep road cuts within the Yellow River canyon, adjacent to the southern Gonghe stratigraphic section (Figs. 2 and 3; Figs. A2 and A3 [see footnote 1]). They yield burial ages of 3.0 ± 2.0 Ma (187 m depth), 3.9 ± 1.3 Ma (271 m depth), and 5.8 ± 0.5 Ma (310 m depth). Given that the half-lives of ^{10}Be and ^{26}Al limit the age range of cosmogenic burial dating to the last ~5 m.y., we consider the deepest sample (NHCOSB0) to indicate only that the sample was buried prior to 5 Ma. Collectively, the burial age samples suggest that in southern Gonghe, the upper part of L3 dates to >5–0.5 Ma. Extrapolating the age-depth trend to the base of the L3 deposits suggests the onset of L3 deposition occurred locally at ca. 6–7 Ma, although the unconformity between L2 and L3 may represent several million years of nondeposition and/or erosion during the early stages of Gonghe Nan Shan range growth.

Sample CT7-11 was collected ~20 km to the northeast of the others, 301 m below the basin fill top. It yields a burial age of 3.8 ± 0.6 Ma. Unfortunately, we were only able to identify one road cut that was sufficiently deep for burial age analysis in this portion of the basin, such that it is difficult to bracket sedimentation rates locally. However, if we assume that the basin fill top is an isochronous marker (at ca. 0.5 Ma), as suggested by the results presented here and those of Craddock et al. (2010), the burial age of CT7-11 implies that mean sedimentation in south-central Gonghe was ~90 m/m.y. Given that the canyon is at least ~600 m deep, and that coarse-grained L3 strata extend from the basin fill top to the canyon floor, this sedimentation rate implies that in south-central Gonghe, coarse-grained alluvium related to the growth of the Gonghe Nan Shan began to accumulate at or prior to ca. 7 Ma.

Rock Magnetism

Based on several observations from demagnetization and rock magnetic experiments, we subdivide our paleomagnetic specimens into three categories that reflect the magnetic mineralogy of the specimens. We interpret the samples to contain a diverse assemblage of magnetic minerals, including hematite, magnetite, titanomagnetite, and/or maghemite and goethite in varying proportions (see Data Repository section 4 for a complete discussion [see footnote 1]). Although specimens appear to contain diverse assemblages of magnetic minerals, the measured natural remnant magnetism (NRM) of the samples was typically restricted to ~10^5–10^6 emu cm^{-3}. We did not attempt to interpret the polarity for a small subset of specimens for two reasons. (1) The stepwise demagnetization behavior for a few sites was too erratic to interpret for some sites. (2) The magnetic inclination and the magnetic declination suggested opposing polarities for some sites. In sum, 14% of specimens from the lower section were uninterpretable, and 13% of specimens from the upper section were not interpretable. The proportion of uninterpretable specimens is fairly typical for magnetostratigraphic analysis of terrestrial strata.

Magnetostratigraphy

The magnetostratigraphy for the upper section exhibits seven normal polarity magnetozones and six reverse polarity magnetozones (Fig. 7). The 33 interpretable sites define the magnetostratigraphy, and an additional five sites were uninterpretable. The difference between the mean normal direction and the antipode of reversed polarity direction (g_0) is small, only ~24°, but the section narrowly fails the reversals test (McFadden and McElhinny, 1990) (Fig. 8; Table 4). This is probably an artifact of the low number of reversed polarity sites, causing an imprecise determination of the mean reverse polarity direction, and the consistency in the magnetization directions suggests that they have been stable since sediment deposition.

The magnetostratigraphy from the lower section exhibits 26 normal polarity zones and 25 reversed polarity zones. The 188 interpretable sites from the lower section define the magnetostratigraphy, and on average, a magnetozone is defined by >4 sites. Thirty additional sites did not yield interpretable polarities. The sites pass the reversals test in both geographic coordinates and tilt-corrected coordinates (Fig. 8; Table 4). The reversals test is categorized as indeterminate because the angle at which the mean directions differ at the 95% confidence level is

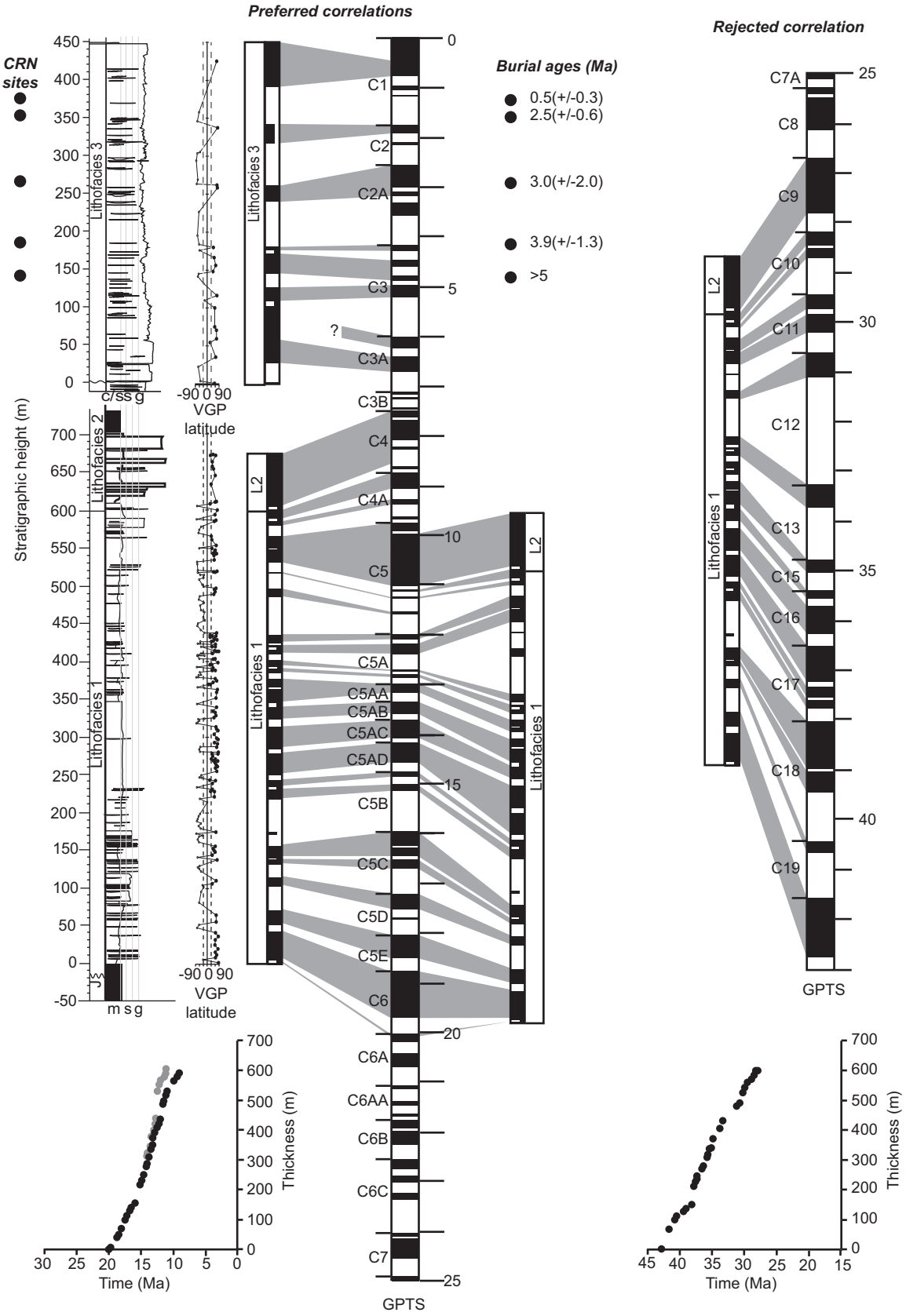

Figure 7. Possible correlations of observed magnetostratigraphy to the geomagnetic polarity time scale (GPTS) of Ogg and Smith (2004). Cryochrons are included in the GPTS. Age in Ma is shown to the right of the GPTS, and chron number is shown to the left of the GPTS. VGP—Virtual geomagnetic pole, CRN—Cosmogenic radionuclide.

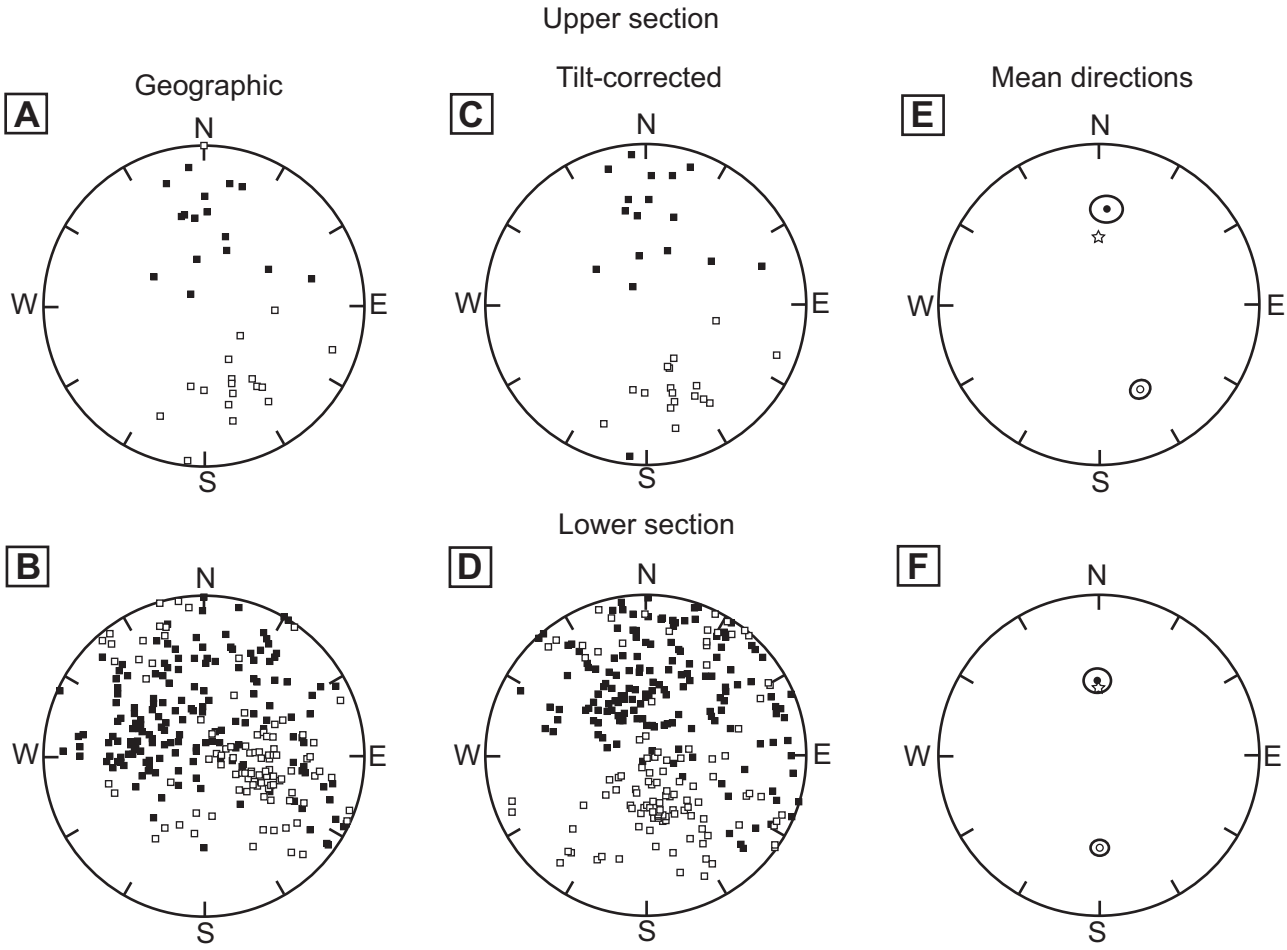

Figure 8. Equal-area plots for lower and upper sections in southern Gonghe, showing (A–B) declination and inclination of all specimens in geographic coordinates, (C–D) declination and inclination for all specimens in tilt-corrected coordinates, and (E–F) mean normal and reversed polarity directions in tilt-corrected coordinates. Solid squares represent lower hemisphere, and open squares represent upper hemisphere. Stars in E–F indicate declination and inclination for sample site, as predicted by the geocentric axial dipole model.

TABLE 4. SUMMARY OF PALEOMAGNETIC DIRECTIONS

Section	Normal polarity				Reversed polarity				Summary statistics		
	Declination	Inclination	N	k	Declination	Inclination	N	k	γ_o	γ_c	Confidence (%)
Geographic coordinates											
Upper Gonghe	4.4	46.6	16	8.5	150.6	–44.6	7	5.2	23.5	16.5	N.A.
Lower Gonghe	310.1	63.3	122	6.6	147.3	–55.3	22	4.9	11.8	22.5	86.5
Tilt-corrected coordinates											
Upper Gonghe	5.2	40.0	16	7.5	153.9	–40.2	7	5.0	23.8	17.3	N.A.
Lower Gonghe	359.3	51.6	122	6.5	179.0	–41.4	22	4.3	10.2	23.3	75.2

Note: N—number of measurements; *k*—precision parameter; γ_o—difference between mean directions; γ_c—threshold above which mean angles differ. See McFadden and McElhinney (1990) and McElhinny and McFadden (2000) for discussion of statistics.

~23° (McFadden and McElhinny, 1990); however, mean directions are very similar, g_0 ~11° (Table 4), suggesting that the mean directions have been stable since deposition.

To assess the resolution of the lower section, we applied a jackknife test (Fig. 9). The lower section has a jackknife statistic of –0.49, which indicates that our sample density recovers at least 95% of the actual magnetozones, and that additional sampling would not reveal a significant number of additional polarity reversals (Tauxe and Gallet, 1991). We note that the inclusion of single-site polarity reversals in our magnetostratigraphy lowers our jackknife statistic. We did not perform the jackknife test on the upper section because the predominance of gravel beds within the section prohibits additional sampling.

Correlation of Magnetostratigraphy to the GPTS

The combination of burial ages and regional biostratigraphy indicates that the coarse-grained alluvium that caps southern Gonghe Basin strata dates to the Pliocene–Pleistocene and provides the basis for correlating the corresponding, low-resolution magnetostratigraphy to the GPTS (Fig. 7). In particular, the two deepest burial age samples, which date to ca. 4–5 Ma and correlate to the section at ~150 m height, suggest that the basal, normal polarity–dominated interval correlates to the upper part of chron 3, which also dates to ca. 4–5 Ma. This correlation implies that locally, gravel deposition in southern Gonghe began at ca. 7 Ma, during chron 3a. The shallowest burial age sample dates to ca. 0.5 Ma and suggests that, like other sections from the region, the top of the section correlates to the upper part of chron 1. The remaining polarity zones in the magnetostratigraphy in the upper part of the Gonghe section were correlated to the GPTS in a way that minimizes erratic fluctuations in sediment accumulation rates and honors thick zones of normal or reversed polarity. Given these guidelines, the thick reversed polarity magnetozones in the middle of the section appear to correlate to the long reversed polarity intervals at the base of chron 1, chron 2, and chron 2a (Fig. 7). The well-ordered stratigraphic succession of burial ages indicates that they are reliable as guides for our magnetostratigraphic correlation.

Although the lower section must be older than the overlying L3 deposits, we lack information that anchors the correlation to the GPTS, so we considered a number of Cenozoic correlations. The thick reversed polarity zones between 430 and 480 m and between 180 and 220 m permit only a few options. Given that the average duration of Neogene polarity chrons is ~0.25 m.y., and that we observe 25 normal and 26 reversed polarity intervals, we sought correlations that span ~13 m.y. (e.g., Lowrie and Kent, 2004). Due to the fact that we incorporated single-site polarity reversals in our magnetostratigraphy, we accepted correlations spanning slightly less time. Given the lack of local constraints on the depositional age of the lower levels of southern Gonghe, we also sought correlations to older intervals of the GPTS (Fig. 7). Importantly, the mean chron duration was longer in the Paleogene than in the Neogene, such that we considered longer Paleogene time windows (Lowrie and Kent, 2004).

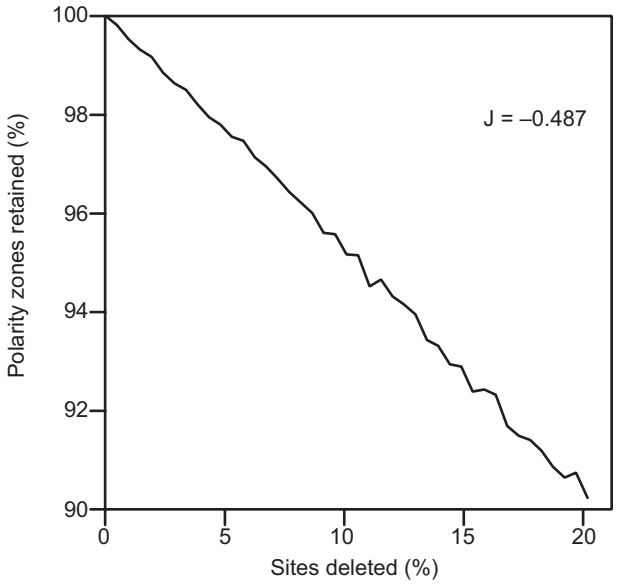

Figure 9. Jackknife test for lower southern Gonghe magnetostratigraphic section. The jackknife statistic, or the slope of the regression line, is better than the recommended limit of –0.5, indicating that additional sampling would not significantly increase the observed number of polarity zones.

We identified two possible correlations to the GPTS, one that spans much of the Miocene and another that spans much of the late Paleogene (Fig. 7). In the Miocene correlation (1a), we link the magnetostratigraphy to the GPTS from C6A to C4. This correlation implies a depositional age of 19.7–ca. 8 Ma, and a duration of sedimentation of ~12 m.y. The correlation implies relatively steady sedimentation rates of ~56 m/m.y. A slight variation of this correlation (1b), in which the long normal polarity zone at the top of our section corresponds to the long normal polarity subchron in C5, is also possible. In this scenario, the top of the section dates to 10.0 Ma, which implies a mean sedimentation rate of ~70 m/m.y. and sediment accumulation over ~10 m.y. In the Paleogene correlation (2), we match our magnetostratigraphy to the portion of the GPTS that spans C20 to C9. This implies a depositional age of 42.8–26.7 Ma and sediment accumulation for ~16 m.y. The implied mean sedimentation rate is ~42 m/m.y.

Three lines of evidence indicate that the Miocene correlation is robust and preferable to the late Paleogene option. This interpretation is consistent with the chronology of lithostratigraphically correlative deposits in adjacent depocenters (Fang et al., 2005; Zhang et al., 2012). First, although a progressive unconformity separates the lower and upper sections, this contact becomes conformable toward the basin center. A similar transition, from fluvial sandstones and mudstones to gravels, is visible in the center of Tongde Basin (Craddock et al., 2010). Here, abundant evidence, including fossils and burial ages (Craddock et al., 2010), indicates that the base of L3 dates to ca. 3.4 Ma. Specifically, a Pliocene fossil was identified just below this stratigraphic transition (QBGMR, 1991). The conformable contact between implies relatively steady sedimentation leading up to gravel deposition, and, therefore, that the younger correlation is probably better. Second, the Miocene correlation implies that sediment accumulation rates were relatively steady, with no major permanent changes in sedimentation rates. Importantly, correlation 1a implies a duration of sediment accumulation of ~12 m.y., which is more consistent with the expected duration of ~13 m.y., than the duration implied by correlation 1b. In contrast, however, the late Paleogene correlation requires pronounced and erratic fluctuations in sediment accumulation rates, particularly between C18 and C17 and C13 and C11 (Fig. 7). Although the Paleogene correlation requires sediment accumulation for ~16 m.y., this may be reasonable given that the mean duration of polarity chrons is longer in the Paleogene than in the Neogene (Lowrie and Kent, 2004). Third, although anomalous polar-

ity zones exist for both correlations, they are less abundant and defined by fewer sites in the Miocene correlation (Fig. 7). Anomalous polarity chrons for the Miocene correlation are typically defined by a single site, whereas five out of eight of the anomalous polarity chrons are defined by multiple sites in the middle Tertiary correlation. Interestingly, the anomalous polarity zones in the Miocene correlation are nearly identical to anomalous polarity zones observed in eastern Qaidam (Fang et al., 2007). Both correlations also omit polarity chrons recorded in the GPTS. In general, due to the depositional hiatuses and minor unconformities that are characteristic of fluvial deposits, magnetostratigraphies of such deposits often omit some short polarity chrons. The Miocene correlation omits 3–5 polarity microchrons (duration of ~0.1 m.y.), which appears to be reasonable given the unsteady nature of sedimentation in fluvial settings. The middle Tertiary correlation omits no polarity chrons, which is to be expected given that the duration of polarity chrons is relatively long in the Paleocene and Eocene (Lowrie and Kent, 2004). Overall, these arguments lead us to prefer the Miocene correlation that places the base of the section at ca. 20 Ma.

IMPLICATIONS

Our preferred magnetostratigraphic correlation, bolstered by cosmogenic burial ages, suggests that the Tertiary deposition in the southern Gonghe Basin initiated in the early Miocene, at ca. 20 Ma, and persisted to ca. 0.5 Ma. Sediment accumulation rates throughout the Miocene appear to have remained relatively steady at ~40–60 m/m.y. Locally, a transition to coarse-grained fluvial and alluvial-fan deposition occurred ca. 7–10 Ma, and may have been time-transgressive away from the Gonghe Nan Shan (e.g., Craddock et al., 2010). The presence of an unconformity at the base of this lithostratigraphic unit (L3) on the northern flank of the range, progressive decrease of bedding dips up section, and growth strata within the unit along the southern range front all suggest that the onset of gravel deposition was associated with the onset of activity along the Gonghe Nan Shan. In this section, we consider the implications of these observations for the evolution of the greater Gonghe region and for the evolution of topography in northeastern Tibet.

Timing, Source, and Cessation of Gravel Deposition around Gonghe Basin Complex

Although global climatic change near the end of the Pliocene has been invoked to explain the deposition of broad sheets of conglomerate in basins around central Eurasia (e.g., Zhang et al., 2001), the time-transgressive nature of gravel deposition in southern Gonghe and Tongde suggests a local tectonic control on conglomerate deposition. The oldest burial ages from southern Gonghe are ≥5 Ma, and in tandem with our magnetostratigraphy, they imply that gravel deposition began at ca. 7 Ma locally. In contrast to southern Gonghe, burial ages, magnetostratigraphy, and fossils from the lowermost gravel deposits in central Tongde Basin date to 3.4 Ma (Craddock et al., 2010). The differences between southern Gonghe and central Tongde suggest that conglomerate deposition initiated earlier on the flanks of the Gonghe Nan Shan than it did in the more distal sections of the basin. Importantly, the burial age from south-central Gonghe also seems to imply that the onset of L3 deposition in the basin center also occurred near the end of the Miocene, perhaps at ca. 7 Ma, although this would suggest relatively rapid progradation of gravel sheets into the basin, on the north side of the Gonghe Nan Shan. The fact that this part of the Gonghe Basin is carried in the hanging wall of the Gonghe Nan Shan faults implies that relatively limited generation of accommodation space may have led to widespread deposition of coarse-grained sediments (e.g., Burbank and Raynolds, 1988). Regardless, our results are consistent with other studies in the Indo-Asian collision zone that suggest that conglomerate deposition is strongly time-transgressive and spans time periods ranging from the mid-Miocene to early Quaternary (e.g., Heermance et al., 2007; Charreau et al., 2009).

Given that deposition of L3 appears to be linked to growth of the Gonghe Nan Shan, one might expect that the volume of L3 deposits would approximate the volume of erosion from the range. However, our structural cross section through the central Gonghe Nan Shan implies a modest amount of structural relief and erosion from within the range, such that the voluminous conglomerate deposits in southern Gonghe and Tongde are somewhat enigmatic. However, conglomerate clast counts imply that a Neogene precursor to the upper Yellow River may have contributed a significant amount of sediment to the basin. Whereas bedrock exposed in the ranges that surround southern Gonghe and Tongde consists of weakly metamorphosed sedimentary rocks, dominantly slate and sandstone/quartzite (QBGMR, 1991), many of the Pliocene–Quaternary (see Craddock et al., 2010; Perrineau et al., 2011) terrace lag deposits associated with the Yellow River display a wide variety of clast compositions (Fig. 5). A local source for many of these clasts cannot be identified. The spatial association of these deposits with the present-day Yellow River implies that this fluvial system played a role in L3 sedimentation along the fringes of the Gonghe Nan Shan, at least during the Pliocene, providing a likely source for the large volume of coarse-grained Pliocene–Pleistocene alluvium within the south-central Gonghe Basin. It is also important to highlight that the cessation of basin filling at ca. 0.5 Ma corroborates recent suggestions that this time marks a transition from basin filling to excavation during an episode of headward erosion by the Yellow River (Craddock et al., 2010).

Tertiary Foreland Basin Development around the NE Tibetan Plateau

The onset of Tertiary sedimentation within the southern Gonghe depocenter has important implications for tectonic reconstructions of the northeastern Tibetan Plateau during the Cenozoic. As described previously, significant depocenters existed in the Xining-Lanzhou region of northeastern Tibet and in western Qaidam by the early Tertiary (e.g., Horton et al., 2004; Dai et al., 2006; Yin et al., 2007; Zhuang et al., 2011) (Fig. 10). The hypothesis that these tectonic elements were linked in a broad foreland during early Tertiary growth of the plateau rests on the similarity in timing between activity along the West Qinling fault, the primary structure that bounds the southern flank of purported foreland sediments (e.g., Fang et al., 2003; Clark et al., 2010; Duvall et al., 2011), and activity along the southern margin of the Qaidam Basin (Clark et al., 2010). As argued herein, our preferred chronology from the southern Gonghe Basin suggests that this basin was not established as a significant depocenter until ca. 20 Ma, and thus our results appear to preclude the hypothesis of a continuous foreland between the Qaidam Basin and northeastern Tibet.

It is notable, however, that several basins in northeastern Tibet began to accumulate sediment in the late Oligocene to early Miocene (Fig. 10). Basins east of Gonghe, including the Guide, Jian Zha, Xunhua, and Linxia Basins (Figs. 1 and 10) all lie to the north-northeast of the West Qinling fault system and south of the Laji Shan. Basal Tertiary sediments in most, if not all, of these basins dates to between ca. 20 and 30 Ma (Fang et al., 2003, 2005; Hough et al., 2011; Lease et al., 2012). In contrast, depocenters to the northwest of our field area are even younger, dating to the later part of the Miocene (Métivier et al., 1998; Fang et al., 2007; Yin et al., 2007; Zhang et al., 2012). Together, these patterns suggest that the locus of Tertiary deposition was not connected to the eastern Qaidam Basin in the early Tertiary (ca. 40 Ma)

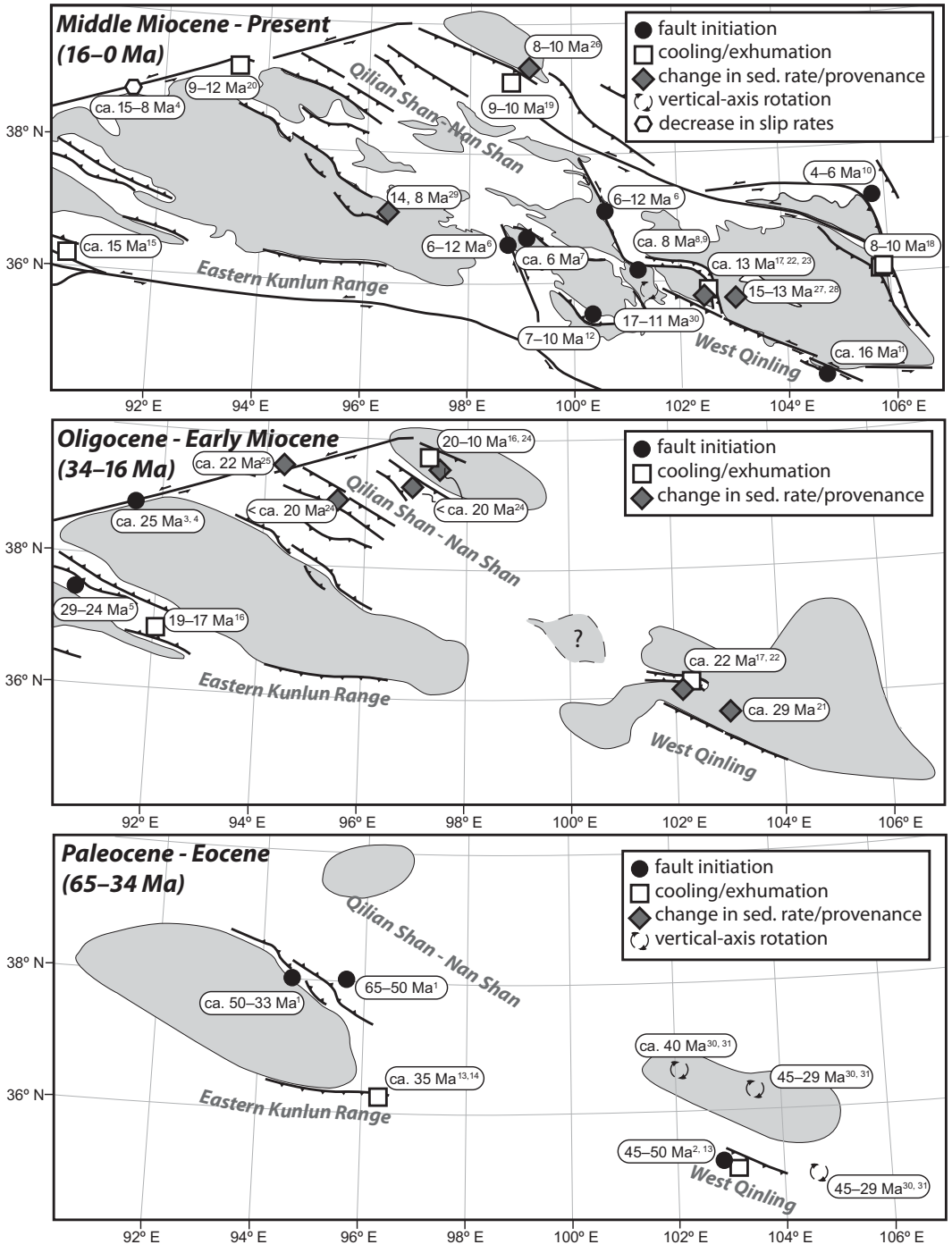

Figure 10. Cenozoic faulting and basin evolution of the northeastern Tibetan Plateau. Fault initiation ages were derived from [1]Yin et al. (2008a); [2]Duvall et al. (2011); [3]Yue et al. (2003); [4]Ritts et al. (2008); [5]Yin et al. (2008b); [6]Yuan et al. (2011); [7]Zhang et al. (2012); [8]Fang et al. (2005); [9]Lease et al. (2007); [10]W. Wang et al. (2011); [11]Z. Wang et al. (2012); and [12]this study. Timing of cooling/exhumation were derived from [13]Clark et al. (2010); [14]Mock et al. (1999); [15]Jolivet et al. (2003); [16]Jolivet et al. (2001); [17]Lease et al. (2011a); [18]Zheng et al. (2006); [19]Zheng et al. (2010); and [20]Wan et al. (2001). Sediment accumulation rate and/or provenance changes were derived from [21]Fang et al. (2003); [22]Lease et al. (2012); [23]Hough et al. (2011); [24]Zhuang et al. (2011); [25]Gilder et al. (2001); [26]Bovet et al. (2009); [27]Garzione et al. (2005); [28]Dettman et al. (2003); and [29]Fang et al. (2007). Vertical-axis rotations are from [30]Dupont-Nivet et al. (2004) and [31]Dupont-Nivet et al. (2008). Sedimentary basins are generalized from Yin et al. (2007) (Qaidam); Zhuang et al. (2011) (northern Qilian/Hexi Corridor region); Horton et al. (2004) (Xining-Lanzhou-Linxia-Guide-Xunhua); Fang et al. (2003, 2005) (Linxia and Guide, respectively); and this study (Gonghe).

but rather that these two regions developed as independent entities.

The geodynamic setting of Oligocene–Miocene basin development in northeastern Tibet remains somewhat enigmatic. Although extensive sedimentation in Guide and southwestern Linxia has been attributed to flexural loading by individual ranges along the Laji-Jishi Shan structural trend (e.g., Fang et al., 2003; Horton et al., 2004), data from northeastern Tibet are starting to suggest that, in many cases, sediment accumulation predated growth of individual ranges (e.g., Fang et al., 2003, 2005; Lease et al., 2007, 2012; Hough et al., 2011) (Fig. 10). This certainly appears to be the case in the southern Gonghe, where growth of the Gonghe Nan Shan appears to have lagged the initial development of the southern Gonghe depocenter by ≥10 m.y. These lags between sediment accumulation and growth of adjacent mountain ranges across the region during the middle Tertiary suggest a role for additional subsidence mechanisms. One possibility is that ponding of sediment may have occurred within a topographically enclosed catchment (Horton et al., 2004). However, it seems equally likely that broad subsidence reflects the development of flexural subsidence associated with an evolving highland to the south. High topography in the Anyemaqen Shan and the Ela Shan, which comprise the southern

and western flanks of the basin complex, may be candidates for a mid-Tertiary highland that could have provided both a source of sediment and a far-field load. Prevalent ESE-directed paleocurrents in pregrowth strata in our measured section provide a hint that the Ela Shan was an important sediment source during the early stages of southern Gonghe basin evolution, but this remains to be tested with detailed stratigraphic data.

Widespread Mountain Building in the Late Miocene

As argued here, emergence and growth of the Gonghe Nan Shan occurred synchronously with deposition of L3 strata. Given that the unconformity separating L2 and L3 appears to bracket the onset of range growth, our preferred chronology implies that range growth initiated at ca. 7–10 Ma. These results extend evidence for coordinated thrust faulting around northeastern Tibet from ca. 12 to 8 Ma, as previously argued by Molnar (2005) (Fig. 10). Activity along the Gonghe Nan Shan at this time is particularly significant for two reasons. First, this is one of the few ranges where growth strata provide a definitive tie between sediment accumulation and fault activity; many other studies rely heavily on stratigraphic and thermochronologic proxies of range growth (Fig. 10). More important, however, is the similarity in the timing of shortening and the growth of the Gonghe Nan Shan with a recent estimate from the northwestern margin of the basin (Zhang et al., 2012), where the initiation of growth along the Qinghai Nan Shan was inferred to have occurred at ca. 6–7 Ma. It appears that both south-vergent thrust systems bounding the greater Gonghe Basin complex were activated in the late Miocene. Moreover, these thrust systems are kinematically associated with northwest-striking, dextral strike-slip faults at both their western (Elashan fault, Fig. 1) and eastern (Riyueshan fault, Fig. 1) tips. Based on an assessment of Pleistocene slip rates (~1 mm/yr) and total displacement (~8–10 km) along these faults, Yuan et al. (2011) suggested that these strike-slip faults also initiated at this time. Collectively, all of these studies suggest that that fault systems around the Gonghe Basin appear to have initiated synchronously. Notably, all of these faults remain active today and suggest that the modern strain field in this region was established in the late Miocene.

From a regional perspective, our results argue in support of the notion that this time period marks a significant reorganization of deformation in northeastern Tibet (e.g., Lease et al., 2011) associated with coordinated range growth (e.g., Molnar, 2005). Ranges along the periphery of the Qilian Shan (Jolivet et al., 2001; Bovet et al., 2009; Zheng et al., 2010) and in northeastern Tibet (Zheng et al., 2006; Lease et al., 2007, 2011; Hough et al., 2011; Wang et al., 2011) all appear to have undergone significant rock uplift and exhumation in the time period 7–13 Ma. Across the Gonghe region, we do not see any evidence for a progressive activation of fault systems during northward growth of the Tibetan Plateau, or, in fact, during southward growth of the Qilian Shan. Such widespread activity, coordinated in time, appears to herald a fundamental change in the kinematics (Royden et al., 2008; Lease et al., 2011), and perhaps the dynamics of deformation throughout northeast Tibet (Molnar, 2005).

CONCLUSIONS

Stratigraphic archives of Tertiary mountain building in the Gonghe Basin complex shed light on the Cenozoic geologic evolution of the interior part of northeastern Tibet, in a transitional region between the Tibetan Plateau, the eastern Qilian Shan, and the northeastern Tibetan Plateau. New chronology from magnetostratigraphy and cosmogenic burial ages, coupled with structural and stratigraphic constraints on the relative timing of sediment accumulation and thrusting along the Gonghe Nan Shan, lead us to the following conclusions:

(1) Our chronology suggests that late Cenozoic sedimentation initiated in the Gonghe region at ca. 20 Ma, and proceeded at rates of ~50–70 m/m.y. until ca. 7–10 Ma. The history of basin evolution across the interior northeastern Tibetan Plateau implies that Eocene–Oligocene basins in the western Qaidam region and near the northeastern plateau margin largely evolved as isolated depocenters, prior to the middle Tertiary. Although the mechanisms underlying widespread subsidence in the early Miocene remain speculative, topographic growth of regions to the south and west of Gonghe may have played an important role (e.g., Clark et al., 2010).

(2) Evolving depositional environments, changing paleocurrents, foreland basin structural architecture, and the presence of growth strata and progressive unconformities reveal the emergence of the Gonghe Nan Shan between 7 and 10 Ma. This observation extends the region of known late Miocene thrust faulting in northeastern Tibet to the interior as well as the periphery of the plateau. Although the dynamics responsible for this expansion of high topography in Tibet are uncertain, the abrupt onset and synchronous range growth across a broad region appear to be consistent with models that invoke a fundamental change in the force balance throughout the orogen (e.g., Molnar, 2005).

(3) Pliocene–Quaternary gravel deposition was time-transgressive around the Gonghe Basin complex of northeastern Tibet. In Gonghe Basin, structural and stratigraphic relationships tie conglomerate deposition to the rise of basin-bounding mountain ranges. Enhanced climate variability since the onset of glacial conditions in the Pliocene does not appear to explain the widespread gravel sheets that blanket Gonghe Basin. Thus, our results lend additional credence to the argument that the onset of coarse-grained sediment accumulation in terrestrial basins throughout Eurasia was time-transgressive (e.g., Heermance et al., 2007; Charreau et al., 2009) and may not record a global climate signal.

ACKNOWLEDGMENTS

This research was supported by the Continental Dynamics program at the U.S. National Science Foundation (EAR-0506622), the National Science Foundation of China (40234040), and the State Key Laboratory of Earthquake Dynamics (China) (LED2008A01). Our thinking was refined by discussions with Doug Burbank, Marin Clark, Alison Duvall, Carmie Garzione, Brian Hough, and Peter Molnar. We thank Richard Lease, Tim Raub, and Isaac Hilburn for assistance with paleomagnetic work, Nate Harkins, Greg Chmiel, and Tom Clifton for assistance with cosmogenic laboratory work, and Xuhua Shi, Ali Sacks, and Jianhui Liu for assistance in the field. Weitao Wang provided assistance translating some references from the Chinese. Kirby gratefully acknowledges support from the Alexander von Humboldt Foundation during construction of this manuscript. Thoughtful reviews by J. Saylor and an anonymous reviewer improved the quality of this manuscript.

REFERENCES CITED

Bovet, P.M., Ritts, B.D., Gehrels, G., Abbink, A.O., Darby, B.J., and Hourigan, J., 2009, Evidence of Miocene crustal shortening in the North Qilian Shan from Cenozoic stratigraphy of the western Hexi Corridor, Gansu Province, China: American Journal of Science, v. 309, p. 290–329, doi:10.2475/00.4009.02.

Burbank, D.W., and Raynolds, R.G.H., 1988, Stratigraphic keys to the timing of thrusting in terrestrial foreland basins: Applications to the northwestern Himalaya, *in* Kleinspahn, K.L., and Paola, C., eds., New Perspectives in Basin Analysis: New York, Springer-Verlag, p. 331–352.

Burchfiel, B.C., Deng, Q., Molnar, P., Royden, L.H., Wang, Y., Zhang, P., and Zhang, W., 1989, Intracrustal detachment within zones of continental deformation: Geology, v. 17, p. 448–452, doi:10.1130/0091-7613(1989)017<0448:IDWZOC>2.3.CO;2.

Charreau, J., Gumiaux, C., Avouac, J.-P., Augier, R., Chen, Y., Barrier, L., Gilder, S., Dominguez, S., Charles, N., and Wang, Q., 2009, The Neogene Xiyu Formation, a diachronous prograding gravel wedge at front of the Tianshan: Climatic and tectonic implications: Earth and Planetary Science Letters, v. 287, no. 3–4, p. 298–310, doi:10.1016/j.epsl.2009.07.035.

Clark, M.K., and Royden, L.H., 2000, Topographic ooze: Building the eastern margin of Tibet by lower crustal flow: Geology, v. 28, no. 8, p. 703–706, doi:10.1130/0091-7613(2000)28<703:TOBTEM>2.0.CO;2.

Clark, M.K., Farley, K.A., Zheng, D., and Duvall, A.R., 2010, Early Cenozoic faulting of the northern Tibetan Plateau margin from apatite (U-Th)/He ages: Earth and Planetary Science Letters, v. 296, no. 1–2, p. 78–88, doi:10.1016/j.epsl.2010.04.051.

Collinson, J.D., 1996, Alluvial sediments, *in* Reading, H.G., ed., Sedimentary Environments: Processes, Facies, and Stratigraphy: Oxford, Blackwell Science, p. 37–82.

Craddock, W.H., Kirby, E., Harkins, N., Zhang, H., Shi, X., and Liu, J., 2010, Rapid fluvial incision along the Yellow River during headward basin integration: Nature Geoscience, v. 3, p. 209–213, doi:10.1038/ngeo777.

Dai, S., Fang, X., Dupont-Nivet, G., Song, C., Gao, J., Krijgsman, W., Langereis, C., and Zhang, W., 2006, Magnetostratigraphy of Cenozoic sediments from the Xining Basin: Tectonic implications for the northeastern Tibetan Plateau: Journal of Geophysical Research, v. 111, B11102, p. 1–19, doi:10.1029/2005JB004187.

Darby, B.J., Ritts, B.D., Yue, Y., and Meng, Q., 2005, Did the Altyn Tagh fault extend beyond the Tibetan Plateau?: Earth and Planetary Science Letters, v. 240, no. 2, p. 425–435, doi:10.1016/j.epsl.2005.09.011.

Davis, M., Matmon, A., Fink, D., Ron, H., and Niedermann, S., 2011, Dating Pliocene lacustrine sediments in the central Jordan valley, Israel—Implications for cosmogenic burial dating: Earth and Planetary Science Letters, v. 305, p. 317–327, doi:10.1016/j.epsl.2011.03.003.

Dayem, K.E., Molnar, P., Clark, M.K., and Houseman, G.A., 2009, Far-field lithospheric deformation in Tibet during continental collision: Tectonics, v. 28, TC6005, p. 1–9, doi:10.1029/2008TC002344.

DeCelles, P.G., Robinson, D.M., and Zandt, G., 2002, Implications of shortening in the Himalayan fold-thrust belt for uplift of the Tibetan Plateau: Tectonics, v. 21, no. 6, doi:10.1029/2001TC001322.

DeCelles, P.G., Quade, J., Kapp, P., Fan, M., Dettman, D.L., and Ding, L., 2007, High and dry in central Tibet during the late Oligocene: Earth and Planetary Science Letters, v. 253, no. 3–4, p. 389–401, doi:10.1016/j.epsl.2006.11.001.

Dettman, D.L., Fang, X., Garzione, C.N., and Li, J., 2003, Uplift-driven climate change at 12 Ma: A long $\delta^{18}O$ record from the NE margin of the Tibetan Plateau: Earth and Planetary Science Letters, v. 214, no. 1–2, p. 267–277, doi:10.1016/S0012-821X(03)00383-2.

Dupont-Nivet, G., Horton, B.K., Butler, R.F., Wang, B., Zhou, J., and Waanders, G.L., 2004, Paleogene clockwise tectonic rotation of the Xining-Lanzhou region, northeastern Tibetan Plateau: Journal of Geophysical Research, v. 109, B04401, doi:10.1029/2003JB002620.

Dupont-Nivet, G., Dai, S., Fang, X., Krijgsman, W., Erens, V., Reitsma, M., and Langereis, C., 2008, Timing and distribution of tectonic rotations in the northeastern Tibetan Plateau, *in* Burchfiel, B.C., and Wang, E., eds., Investigations into the Tectonics of the Tibetan Plateau: Geological Society of America Special Paper 444, p. 73–87, doi:10.1130/2008.2444(05).

Dupont-Nivet, G., Lippert, P.C., Van Hinsbergen, D.J.J., Meijers, M.J.M., and Kapp, P., 2010, Paleolatitude and age of the Indo-Asia collision: Paleomagnetic constraints: Geophysical Journal International, v. 182, no. 3, p. 1189–1198, doi:10.1111/j.1365-246X.2010.04697.x.

Duvall, A.R., Clark, M.K., van der Pluijm, B.A., and Li, C., 2011, Direct dating of Eocene reverse faulting in northeastern Tibet using Ar-dating of fault clays and low-temperature thermochronometry: Earth and Planetary Science Letters, v. 304, no. 3–4, p. 520–526, doi:10.1016/j.epsl.2011.02.028.

England, P., and Houseman, G.A., 1986, Finite strain calculations of continental deformation: 2. Comparison with the India-Asia collision zone: Journal of Geophysical Research, v. 91, no. B3, p. 3664–3676, doi:10.1029/JB091iB03p03664.

Fang, X., Garzione, C.N., Van der Voo, R., Li, J., and Fan, M., 2003, Flexural subsidence by 29 Ma on the NE edge of Tibet from magnetostratigraphy of Linxia Basin, China: Earth and Planetary Science Letters, v. 210, no. 3–4, p. 545–560, doi:10.1016/S0012-821X(03)00142-0.

Fang, X., Yan, M., Van der Voo, R., Rea, D.K., Song, C., Pares, J.M., Gao, J., Nie, J., and Dai, S., 2005, Late Cenozoic deformation and uplift of the NE Tibetan Plateau: Evidence from high-resolution magnetostratigraphy of the Guide Basin, Qinghai Province, China: Geological Society of America Bulletin, v. 117, no. 9–10, p. 1208–1225, doi:10.1130/B25727.1.

Fang, X., Zhang, W., Meng, Q., Gao, J., Wang, X., King, J., Song, C., Dai, S., and Miao, Y., 2007, High-resolution magnetostratigraphy of the Neogene Huaitoutala section in the eastern Qaidam Basin on the NE Tibetan Plateau, Qinghai Province, China, and its implications on the tectonic uplift of the NE Tibetan Plateau: Earth and Planetary Science Letters, v. 258, no. 1–2, p. 293–306, doi:10.1016/j.epsl.2007.03.042.

Garzanti, E., and van Haver, T., 1988, The indus clastics: Forearc basin sedimentation in the Ladakh Himalaya (India): Sedimentary Geology, v. 59, no. 3–4, p. 237–249, doi:10.1016/0037-0738(88)90078-4.

Garzione, C.N., Ikari, M.J., and Basu, A., 2005, Source of Oligocene to Pliocene sedimentary rocks in the Linxia Basin in northeastern Tibet from Nd isotopes: Implications for tectonic forcing of climate: Geological Society of America Bulletin, v. 117, no. 9/10, p. 1156–1166, doi:10.1130/B25743.1.

George, A.D., Marshallsea, S.J., Wyrwoll, K.-H., Chen, J., and Lu,Y., 2001, Miocene cooling in the northern Qilian Shan, northeastern margin of the Tibetan Plateau, revealed by apatite fission-track and vitrinite-reflectance analysis: Geology, v. 29, no. 10, p. 939–942, doi:10.1130/0091-7613(2001)029<0939:MCITNQ>2.0.CO;2.

Gilder, S., Chen, Y., and Sen, S., 2001, Oligo-Miocene magnetostratigraphy and rock magnetism of the Xishuigou section, Subei (Gansu Province, western China) and implications for shallow inclinations in central Asia: Journal of Geophysical Research, v. 106, no. 12, p. 30,505–30,521, doi:10.1029/2001JB000325.

Granger, D.E., 2006, A review of burial dating methods using ^{10}Be and ^{26}Al, *in* Siame, L.L., Bourles, D.L., and Brown, E.T., eds., In Situ–Produced Cosmogenic Nuclides and Quantification of Geological Processes: Geological Society of America Special Paper 415, p. 1–16.

Granger, D. E., and Muzikar, P. F., 2001, Dating sediment burial with in situ–produced cosmogenic nuclides: Theory, techniques, and limitations: Earth and Planetary Science Letters, v. 188, no. 1–2, p. 269–281, doi:10.1016/S0012-821X(01)00309-0.

Granger, D.E., Kirchner, J.W., and Finkel, R.C., 1997, Quaternary downcutting rate of the New River, Virginia, measured from differential decay of cosmogenic ^{26}Al and ^{10}Be in cave-deposited alluvium: Geology, v. 25, no. 2, p. 107–110, doi:10.1130/0091-7613(1997)025<0107:QDROTN>2.3.CO;2.

Harkins, N., Kirby, E., Heimsath, A., Robinson, R., and Reiser, U., 2007, Transient fluvial incision in the headwaters of the Yellow River, northeastern Tibet, China: Journal of Geophysical Research, v. 112, F03S04, doi:10.1029/2006JF000570.

Harkins, N., Kirby, E., Shi, X., Wang, E., Burbank, D.W., and Chun, F., 2010, Millennial slip rates along the eastern Kunlun fault: Implications for the dynamics of intracontinental deformation in Asia: Lithosphere, v. 2, no. 4, p. 247–266, doi: 1130/L85.1.

Harms, J.C., Southard, J.B., and Walker, R.G., 1982, Structures and sequences in clastic rocks: Society of Economic Paleontologists and Mineralogists Short Course Notes, v. 9, p. 2-1–2-55, doi: 10.2110/scn.82.09.0000.

Heermance, R.V., Chen, J., Burbank, D.W., and Wang, C., 2007, Chronology and tectonic controls of late Tertiary deposition in the southwestern Tian Shan foreland, NW China: Basin Research, v. 19, no. 4, p. 599–632, doi:10.1111/j.1365-2117.2007.00339.x.

Horton, B.K., Dupont-Nivet, G., Zhou, J., Waanders, G.L., Butler, R.F., and Wang, J., 2004, Mesozoic–Cenozoic evolution of the Xining-Minhe and Dangchang Basins, northeastern Tibetan Plateau: Magnetostratigraphic and biostratigraphic results: Journal of Geophysical Research, v. 109, B04402, p. 1–15, doi:10.1029/2003JB002913.

Hough, B.G., Garzione, C.N., Wang, Z., Lease, R.O., Burbank, D.W., and Yuan, D., 2011, Stable isotope evidence for topographic growth and basin segmentation: Implications for the evolution of the NE Tibetan Plateau: Geological Society of America Bulletin, v. 123, no. 1–2, p. 168–185, doi: 10.1130.B30090.1.

Jolivet, M., Brunel, M., Seward, D., Xu, Z., Yang, J., Roger, F., Tapponnier, P., Malavieille, J., Arnaud, N., and Wu, C., 2001, Mesozoic and Cenozoic tectonics of the northern edge of the Tibetan Plateau: Fission-track constraints: Tectonophysics, v. 343, no. 1–2, p. 111–134, doi:10.1016/S0040-1951(01)00196-2.

Jolivet, M., Brunel, M., Seward, D., Xu, Z., Yang, J., Malavieille, J., Roger, F., Leyreloup, A., Arnaud, N., and Wu, C., 2003, Neogene extension and volcanism in the Kunlun fault zone, northern Tibet: New constraints on the age of the Kunlun fault: Tectonics, v. 22, no. 5, p. 7–1–7–23, doi:10.1029/2002TC001428.

Jones, C.H., 2002, User-driven integrated software live: "PaleoMag" paleomagnetics analysis on the Macintosh: Computers & Geosciences, v. 28, no. 10, p. 1145–1151, doi:10.1016/S0098-3004(02)00032-8.

Kapp, P., Yin, A., Harrison, T.M., and Ding, L., 2005, Cretaceous–Tertiary shortening, basin development, and volcanism in central Tibet: Geological Society of America Bulletin, v. 117, no. 7/8, p. 865–878, doi:10.1130/B25595.1.

Kent-Corson, M.L., Ritts, B.D., Zhuang, G., Bovet, P.M., Graham, S.A., and Chamberlain, C.P., 2009, Stable isotopic constraints on the tectonic, topographic, and climatic evolution of the northern margin of the Tibetan Plateau: Earth and Planetary Science Letters, v. 282, no. 1–4, p. 158–166, doi:10.1016/j.epsl.2009.03.011.

Kirschvink, J.L., 1980, The least-squares line and plane and the analysis of palaeomagnetic data: Geophysical Journal of the Royal Astronomical Society, v. 62, no. 3, p. 699–718.

Lease, R.O., Burbank, D.W., Gehrels, G., Wang, Z., and Yuan, D., 2007, Signatures of mountain building: Detrital zircon U/Pb ages from northeastern Tibet: Geology, v. 35, no. 3, p. 239–242, doi:10.1130/G23057A.1.

Lease, R.O., Burbank, D.W., Clark, M.K., Farley, K.A., Zheng, D., and Zhang, H., 2011, Middle Miocene reorganization of deformation along the northeastern Tibetan Plateau: Geology, v. 39, no. 4, p. 359–362, doi:10.1130/G31356.1.

Lease, R.O., Burbank, D.W., Hough, B., Wang, Z., and Yuan, D., 2012, Pulsed Miocene range growth in northeastern Tibet: Insights from Xunhua Basin magnetostratigraphy: Geological Society of America Bulletin (in press).

Lippert, P.C., Zhao, X., Coe, R.S., and Lo, C.-H., 2010, Paleomagnetism and $^{40}Ar/^{39}Ar$ geochronology of upper Paleaogene volcanic rocks from central Tibet: Implications for the central Asia inclination anomaly, the palaeolatitude of Tibet and post–50 Ma shortening within Asia: Geophysical Journal International, v. 184, no. 1, p. 131–161, doi:10.1111/j.1365-246X.2010.04833.x.

Lowrie, W., and Kent, D.V., 2004, Geomagnetic polarity timescales and reversal frequency regimes, *in* Channell, J., Kent, D., Lowrie, W., and Meert, J., eds., Time Scales of the Paleomagnetic Field: American Geophysical Union Geophysical Monograph 145, p. 117–129.

McElhinny, M.W., and McFadden, P.W., 2000, Paleomagnetism: Continents and Oceans: New York, Academic Press, 382 p.

McFadden, P.L., and McElhinny, M.W., 1990, Classification of the reversals test in palaeomagnetism: Geophysical Journal International, v. 103, p. 725–729, doi:10.1111/j.1365-246X.1990.tb05683.x.

Meng, Q.-R., Hu, J.-M., Jin, J.-Q., Zhang, Y., and Xu, D.-F., 2003, Tectonics of the late Mesozoic wide extensional basin system in the China-Mongolia border region: Basin Research, v. 15, p. 397–415, doi:10.1046/j.1365-2117.2003.00209.x.

Métivier, F., Gaudemer, Y., Tapponnier, P., and Meyer, B., 1998, Northeastward growth of the Tibet Plateau deduced from balanced reconstruction of two depositional areas: The Qaidam and Hexi Corridor basins, China: Tectonics, v. 17, no. 6, p. 823–842, doi:10.1029/98TC02764.

Meyer, B., Tapponnier, P., Bourjot, L., Métivier, F., Gaudemer, Y., Peltzer, G., Shunmin, G., and Zhitai, C., 1998, Crustal thickening in Gansu-Qinghai, lithospheric mantle subduction, and oblique, strike-slip controlled growth of the Tibet Plateau: Geophysical Journal International, v. 135, no. 1, p. 1–47, doi:10.1046/j.1365-246X.1998.00567.x.

Miall, A.D., 1996, The Geology of Fluvial Deposits: Sedimentary Facies, Basin Analysis, and Petroleum Geology: New York, Springer, 582 p.

Miall, A.D., 2000, Principles of Sedimentary Basin Analysis: New York, Springer, 616 p.

Mock, C., Arnaud, N.O., and Cantagrel, J.-M., 1999, An early unroofing in northeastern Tibet? Constraints from $^{40}Ar/^{39}Ar$ thermochronology on granitoids from the eastern Kunlun range (Qianghai, NW China): Earth and Planetary Science Letters, v. 171, p. 107–122, doi:10.1016/S0012-821X(99)00133-8.

Molnar, P., 2005, Mio-Pliocene growth of the Tibetan Plateau and evolution of East Asian climate: Palaeontologia Electronica, v. 8, no. 1, p. 1–23.

Molnar, P., and Stock, J.M., 2009, Slowing of India's convergence with Eurasia since 20 Ma and its implications for Tibetan mantle dynamics: Tectonics, v. 28, TC3001, doi:10.1029/2008TC002271.

Molnar, P., and Tapponnier, P., 1978, Active tectonics of Tibet: Journal of Geophysical Research, v. 83, no. B11, p. 5361–5375, doi:10.1029/JB083iB11p05361.

Molnar, P., England, P., and Martinod, J., 1993, Mantle dynamics, uplift of the Tibetan Plateau, and the Indian monsoon: Reviews of Geophysics, v. 31, no. 4, p. 357–396, doi:10.1029/93RG02030.

Murphy, M.A., Yin, A., Harrison, T.M., Dürr, S.B., Chen, Z., Ryerson, F.J., Kidd, W.S.F., Wang, X., and Zhou, X., 1997, Did the Indo-Asian collision alone create the Tibetan Plateau: Geology, v. 25, no. 8, p. 719–722, doi:10.1130/0091-7613(1997)025<0719:DTIACA>2.3.CO;2.

Najman, Y., Appel, E., Boudagher-Fadel, M., Bown, P., Carter, A., Garzanti, E., Godin, L., Han, J., Liebke, U., Oliver, G., Parrish, R., and Vezzoli, G., 2010, Timing of India-Asia collision: Geological, biostratigraphic, and palaeomagnetic results: Journal of Geophysical Research, v. 115, B12416, doi:10.1029/2010JB007673.

Nemec, W., and Postma, G., 1993, Quaternary alluvial fans in southwestern Crete: Sedimentation processes and geomorphic evolution, *in* Marzo, M., and Puigdefabregas, C., eds., Alluvial Sedimentation: International Association of Sedimentologists Special Publication 17, p. 1–31.

Nemec, W., and Steel, R.J., 1984, Alluvial and coastal conglomerates: Their significant features and some comments on gravelly mass-flow deposits, *in* Koster, E.H., and Steel, R.J., eds., Sedimentology of Gravels and Conglomerates: Canadian Society of Petroleum Geologists Memoir 10, p. 1–31.

Ogg, J.G., and Smith, A.G., 2004, The geomagnetic polarity time scale, *in* Gradstein, F.M., Ogg, J.G., and Smith, A.G., eds., A Geologic Time Scale: Cambridge, UK, Cambridge University Press, 589 p.

Patriat, P., and Achache, J., 1984, India-Eurasia collision chronology has implications for crustal shortening and driving mechanisms of plates: Nature, v. 311, p. 615, doi:10.1038/311615a0.

Perrineau, A., Van Der Woerd, J., Gaudemer, Y., Jing, L.Z., Pik, R., Tapponier, P., Thuizat, R., and Zheng, R., 2011, Incision rate of the Yellow River in northeastern Tibet constrained by ^{10}Be and ^{26}Al cosmogenic isotope dating of fluvial terraces: Implications for catchment evolution and plateau building, *in* Gloaguen, R., and Ratschbacher, L., eds., Growth and Collapse of the Tibetan Plateau: Geological Society of London Special Publication 353, p. 189–219.

Qinghai Bureau of Geology and Mineral Resources (QBGMR), 1991, Regional Geology of Qinghai Province: Beijing, Geological Publishing House, 662 p.

Ritts, B.D., Yue, Y., and Graham, S.A., 2004, Oligocene–Miocene tectonics and sedimentation along the Altyn Tagh fault, northern Tibetan Plateau: Analysis of the Xorkol, Subei, and Aksay Basins: The Journal of Geology, v. 112, no. 2, p. 207–229, doi:10.1086/381658.

Ritts, B.D., Yue, Y., Graham, S.A., Sobel, E.R., Abbink, O.A., and Stockli, D.F., 2008, From sea level to high elevation in 15 million years: Uplift history of the northern Tibetan Plateau margin in the Altun Shan: American Journal of Science, v. 308, p. 657–678, doi:10.2475/05.2008.01.

Rowley, D.B., 1996, Age of initiation between India and Asia: A review of stratigraphic data: Earth and Planetary Science Letters, v. 145, p. 1–13, doi:10.1016/S0012-821X(96)00201-4.

Rowley, D.B., and Currie, B.S., 2006, Palaeo-altimetry of the late Eocene to Miocene Lunpola Basin, central Tibet: Nature, v. 439, p. 677–681, doi:10.1038/nature04506.

Royden, L.H., Burchfiel, B.C., and van der Hilst, R.D., 2008, The geological evolution of the Tibetan Plateau: Science, v. 321, no. 5892, p. 1054–1058, doi:10.1126/science.1155371.

Singh, I.B., 1972, On the bedding in the natural-levee and the point-bar deposits of the Gomti River, Uttar Pradesh, India: Sedimentary Geology, v. 7, p. 309–317, doi:10.1016/0037-0738(72)90028-0.

Sobel, E.R., Hilley, G.E., and Strecker, M., 2003, Formation of internally drained contractional basins by aridity-limited bedrock incision: Journal of Geophysical Research, v. 108, no. B7, p. 1–23, doi:10.1029/2002JB001883.

Strecker, M.R., Alonso, R., Bookhagen, B., Carrapa, B., Hilley, G.E., Sobel, E.R., and Trauth, M.H., 2007, Tectonics and climate of the southern central Andes: Annual Review of Earth and Planetary Sciences, v. 35, p. 747–787, doi:10.1146/annurev.earth.35.031306.140158.

Tapponnier, P., and Molnar, P., 1977, Active faulting and tectonics of China: Journal of Geophysical Research, v. 82, no. 20, p. 2905–2930, doi:10.1029/JB082i020p02905.

Tapponnier, P., Meyer, B., Avouac, J.P., Peltzer, G., Gaudemer, Y., Guo, S., Xiang, H., Yin, K., Chen, Z., Cai, S., and Dai, H., 1990, Active thrusting and folding in the Qilian Shan, and decoupling between upper crust and mantle in northeastern Tibet: Earth and Planetary Science Letters, v. 97, no. 3–4, p. 382–383, 387–403, doi:10.1016/0012-821X(90)90053-Z.

Tapponnier, P., Zhiqin, X., Roger, F., Meyer, B., Arnaud, N., Wittlinger, G., and Yang, J., 2001, Oblique stepwise rise and growth of the Tibet Plateau: Science, v. 294, no. 5547, p. 1671–1677, doi:10.1126/science.105978.

Tauxe, L., and Gallet, Y., 1991, A jackknife for magnetostratigraphy: Geophysical Research Letters, v. 18, no. 9, p. 1783–1786, doi: 10.1029/91GL01223.

Tucker, M.E., 2003, Sedimentary Rocks in the Field (3rd ed.): West Sussex, UK, Jon Wiley and Sons, Ltd., 234 p.

Vergne, J., Wittlinger, G., Hui, Q., Tapponnier, P., Poupinet, G., Mei, J., Herquel, G., and Paul, A., 2002, Seismic evidence for stepwise thickening of crust across the NE Tibetan Plateau: Earth and Planetary Science Letters, v. 203, p. 25–33, doi:10.1016/S0012-821X(02)00853-1.

Vincent, S.J., and Allen, M.B., 1999, Evolution of the Minle and Chaoshui Basins, China: Implications for Mesozoic strike-slip basin formation in central Asia: Geological Society of America Bulletin, v. 111, no. 5, p. 725–742, doi:10.1130/0016-7606(1999)111<0725:EOTMAC>2.3.CO;2.

Wan, J., Wang, Y., Li, Q., and Wang, E., 2001, FT evidence of northern Altyn Tagh uplift in the late Cenozoic: Bulletin of Mineralogy, Petrology, and Geochemistry, v. 20, p. 222–224.

Wang, E., Xu, F.-Y., Zhou, J.-X., Wan, J., and Burchfiel, B.C., 2006, Eastward migration of the Qaidam Basin and its implications for Cenozoic evolution of the Altyn Tagh fault and associated river systems: Geological Society of America Bulletin, v. 118, no. 3–4, p. 349–365, doi:10.1130/B25778.1.

Wang, W.-T., Zhang, P.-Z., Kirby, E., Wang, L.-H., Zhang, G.-L., Zheng, D.-W., and Chai, C.-Z., 2011, A revised chronology for Tertiary sedimentation in the Sikouzi Basin: Implications for the tectonic evolution of the northeastern corner of the Tibetan Plateau: Tectonophysics, v. 505, no. 1–4, p. 100–114, doi:10.1016/j.tecto.2011.04.006.

Wang, Z., Zhang, P., Garzione, C.N., Lease, R.O., Zhang, G., Zheng, D., Hough, B., Yuan, D., Li, C., Liu, J., and Wu, Q., 2012, Magnetostratigraphy and depositional history of the Miocene Wushan Basin on the NE Tibetan Plateau, China: Implications for middle Miocene tectonics of the West Qinling fault zone: Journal of Asian Earth Sciences (in press).

Xiao, W., Windley, B.F., Yong, Y., Yan, Z., Yuan, C., Liu, C., and Li, J., 2009, Early Paleozoic to Devonian multiple-accretionary model for the Qilian Shan, NW China: Journal of Asian Earth Sciences, v. 35, p. 323–333, doi:10.1016/j.jseaes.2008.10.001.

Yin, A., and Harrison, T.M., 2000, Geological evolution of the Himalayan-Tibetan orogen: Annual Review of Earth and Planetary Sciences, v. 28, p. 211–280, doi:10.1146/annurev.earth.28.1.211.

Yin, A., Dang, Y.-Q., Zhang, M., McRivette, M.W., Burgess, W.P., and Chen, X.-H., 2007, Cenozoic tectonic evolution of Qaidam Basin and its surrounding regions (part 2): Wedge tectonics in southern Qaidam Basin and the Eastern Kunlun Range, *in* Sears, J.W., Harms, T.A., and Evenchick, C.A., eds., Whence the Mountains? Inquiries into the Evolution of Orogenic Systems: A Volume in Honor of Raymond A. Price: Geological Society of America Special Paper 433, p. 369–390, doi:10.1130/2007.2433(18).

Yin, A., Dang, Y.-Q., Wang, L.-C., Jiang, W.-M., Zhou, S.-P., Chen, X.-H., Gehrels, G.E., and McRivette, M.W., 2008a, Cenozoic tectonic evolution of Qaidam Basin and its surrounding regions (part 1): The southern Qilian Shan–Nan Shan thrust belt and northern Qaidam Basin: Geological Society of America Bulletin, v. 120, no. 7/8, p. 813–846, doi: 10.1130.B26180.1.

Yin, A., Dang, Y.-Q., Zhang, M., Chen, M., Chen, X.-H., and McRivette, M.W., 2008b, Cenozoic tectonic evolution of the Qaidam Basin and its surrounding regions (part 3): Structural geology, sedimentation, and regional tectonic reconstruction: Geological Society of America Bulletin, v. 120, no. 7/8, p. 847–876, doi:10.1130/B26232.1.

Yuan, D., Champagnac, J. D., Ge, W.-P., Molnar, P., Zhang, P.-Z., Zheng, W.-J., Zhang, H.-P., and Liu, X.-W., 2011, Late Quaternary right-lateral slip rates of faults adjacent to the lake Qinghai, northeastern margin of the Tibetan Plateau: Geological Society of America Bulletin, v. 123, no. 9–10, p. 2016–2030, doi:10.1130/B30315.1.

Yue, Y., Ritts, B.D., Graham, S.A., Wooden, J.L., Gehrels, G., and Zhang, Z., 2003, Slowing extrusion tectonics: Lowered estimate of post–early Miocene slip rate for the Altyn Tagh fault: Earth and Planetary Science Letters, v. 217, no. 1–2, p. 111–122, doi:10.1016/S0012-821X(03)00544-2.

Zhang, H.-P., Craddock, W.H., Lease, R.O., Wang, W.-T., Yuan, D.-Y., Zhang, P.-Z., Molnar, P., Zheng, D.-W., and Zheng, W.-J., 2012, Magnetostratigraphy of the Neogene Chaka Basin and its implications for mountain building processes in the north-eastern Tibetan Plateau: Basin Research (in press).

Zhang, P., Molnar, P., and Downs, W.R., 2001, Increased sedimentation rates and grain sizes 2–4 Myr ago due to the influence of climate change on erosion rates: Nature, v. 410, p. 891–897, doi:10.1038/35069099.

Zheng, D., Zhang, P., Wan, J., Li, C., and Cao, J., 2003, Late Cenozoic deformation subsequence in northeastern margin of Tibet: Science in China, v. 46, no. 266–275.

Zheng, D., Zhang, P., Wan, J., Yuan, D., Li, C., Yin, G., Zhang, G., Wang, Z., Min, W., and Chen, J., 2006, Rapid exhumation at ~8 Ma on the Liupan Shan thrust fault from apatite fission-track thermochronology: Implications for growth of the northeastern Tibetan Plateau margin: Earth and Planetary Science Letters, v. 248, no. 1–2, p. 198–208, doi:10.1016/j.epsl.2006.05.023.

Zheng, D., Clark, M.K., Zhang, P., Zheng, W.J., and Farley, K.A., 2010, Erosion, fault initiation and topographic growth of the North Qilian Shan (northern Tibetan Plateau): Geosphere, v. 6, no. 6, p. 937–941, doi:10.1130/GES00523.1.

Zheng, S.H., Wu, W.Y., Li, Y., and Wang, G.D., 1985, Late Cenozoic mammalian faunas of Guide and Gonghe Basins, Qinghai Province: Vertabrata PalAsiatica, v. 23, no. 2, p. 89–134.

Zhuang, G., Hourigan, J.K., Ritts, B.D., and Kent-Corson, M.L., 2011, Cenozoic multiple-phase tectonic evolution of the northern Tibetan Plateau: Constraints from sedimentary records from Qaidam Basin, Hexi Corridor, and Subei Basin, northwest China: American Journal of Science, v. 311, p. 116–152, doi:10.2475/02.2011.02.

MANUSCRIPT RECEIVED 7 JUNE 2011
REVISED MANUSCRIPT RECEIVED 21 OCTOBER 2011
MANUSCRIPT ACCEPTED 25 OCTOBER 2011

Printed in the USA